Accepted Manuscript

Whole genome RNAi screens reveal a critical role of REV3 in coping with replication stress

Ilya N. Kotov, Ellen Siebring - van Olst, Philip A. Knobel, Ida H. van der Meulen-Muileman, Emanuela Felley-Bosco, Victor W. van Beusechem, Egbert F. Smit, Rolf A. Stahel, Thomas M. Marti

PII: S1574-7891(14)00163-X

DOI: 10.1016/j.molonc.2014.07.008

Reference: MOLONC 551

To appear in: *Molecular Oncology*

Received Date: 8 January 2014

Revised Date: 10 July 2014

Accepted Date: 11 July 2014

Please cite this article as: Kotov, I.N., Siebring - van Olst, E., Knobel, P.A., van der Meulen-Muileman, I.H., Felley-Bosco, E., van Beusechem, V.W., Smit, E.F., Stahel, R.A., Marti, T.M., Whole genome RNAi screens reveal a critical role of REV3 in coping with replication stress, *Molecular Oncology* (2014), doi: 10.1016/j.molonc.2014.07.008.

Highlights

- Whole-genome RNAi synthetic sickness/lethality screens were performed.
- We identified synthetic sickness/lethality interaction of RRM1 with REV3.
- HU and iREV3 treatments synergistically induce single-stranded DNA in S-phase.
- This increase is not accompanied by accumulation of DNA damage.
- Our findings indicate that REV3 plays a role in coping with DNA replication stress.

Whole genome RNAi screens reveal a critical role of REV3 in coping with replication stress

Ilya N. Kotov[a], Ellen Siebring - van Olst[b], Philip A. Knobel[a1], Ida H. van der Meulen-Muileman[c], Emanuela Felley-Bosco[a], Victor W. van Beusechem[c], Egbert F. Smit[b], Rolf A. Stahel[a] and Thomas M. Marti[a2]*

[a] Clinic of Oncology, University Hospital Zurich, 8044 Zurich, Switzerland

[b] Department of Pulmonary Diseases and [c] Department of Medical Oncology, VU University Medical Center, 1081 HV Amsterdam, the Netherlands

* Corresponding author. Department of Clinical Research, University Hospital Bern, 3010 Bern, Switzerland; Clinic of Thoracic Surgery, University Hospital Bern, 3010 Bern, Switzerland. Tel: +41 31 632 40 81. Email: thomas.marti@insel.ch

[1] Present address: Institute for Research in Biomedicine, 08028 Barcelona, Spain
[2] Present address: Department of Clinical Research, University Hospital Bern, 3010 Bern, Switzerland; Clinic of Thoracic Surgery, University Hospital Bern, 3010 Bern, Switzerland.

ABSTRACT

REV3, the catalytic subunit of translesion polymerase zeta (polζ), is commonly associated with DNA damage bypass and repair. Despite sharing accessory subunits with replicative polymerase δ, very little is known about the role of polζ in DNA replication. We previously demonstrated that inhibition of REV3 expression induces persistent DNA damage and growth arrest in cancer cells. To reveal determinants of this sensitivity and obtain insights into the cellular function of REV3, we performed whole human genome RNAi library screens aimed at identification of synthetic lethal interactions with REV3 in A549 lung cancer cells. The top confirmed hit was RRM1, the large subunit of ribonucleotide reductase (RNR), a critical enzyme of *de novo* nucleotide synthesis. Treatment with the RNR-inhibitor hydroxyurea (HU) synergistically increased the fraction of REV3-deficient cells containing single stranded DNA (ssDNA) as indicated by an increase in replication protein A (RPA). However, this increase was not accompanied by accumulation of the DNA damage marker γH2AX suggesting a role of REV3 in counteracting HU-induced replication stress (RS). Consistent with a role of REV3 in DNA replication, increased RPA staining was confined to HU-treated S-phase cells. Additionally, we found genes related to RS to be significantly enriched among the top hits of the synthetic sickness/lethality (SSL) screen further corroborating the importance of REV3 for DNA replication under conditions of RS.

Keywords: REV3, polymerase zeta, replication stress, translesion synthesis, DNA damage
Abbreviations: ANOVA, analysis of variance; CDDP, cisplatin; DDR, DNA damage response; HU, hydroxyurea; Polζ, polymerase zeta; RNR, ribonucleotide reductase; RPA, replication protein A; RS, replication stress; ssDNA, single-stranded DNA; SSL, synthetic sickness/lethality; TLS, translesion synthesis

1. Introduction

Integrity and fidelity of the genomic material is constantly compromised in various ways but cells possess multiple mechanisms to cope with it (Jackson and Bartek, 2009). If DNA damage cannot be repaired, it can be tolerated in order to continue replication without formation of lethal intermediates. Translesion synthesis (TLS) is a key DNA damage tolerance pathway that allows bypass of different types of lesions. Dependent on the nature of the lesion and recruited enzymes, this process can result in faithful or error-prone, i.e. mutagenic, DNA replication (reviewed in (Knobel and Marti, 2011)).

Polymerase zeta (polζ), with its catalytic subunit REV3L (hereafter REV3), plays a unique role in TLS. REV3 is able to contribute to mutagenesis in two ways: by introducing mismatches or by extending from a mismatch introduced by another polymerase. Besides, in contrast to other TLS polymerases, REV3 belongs to the B-family and its knockout is embryonic lethal in mice (Esposito et al., 2000; Wittschieben et al., 2000). Despite the development of conditional knockout mice models, (Lange et al., 2013; Wittschieben et al., 2010) the molecular basis for this developmental significance still remains elusive. Apart from its function in TLS, polζ is known to play a role in homologous recombination (Sharma et al., 2012), non-homologous end-joining (Covo et al., 2009) and inter- and intrastrand crosslink repair (Enoiu et al., 2012; Hicks et al., 2010). Additionally, yeast polζ is able to replicate undamaged DNA (Northam et al., 2010) and shares accessory subunits with polymerase δ (Johnson et al., 2012; Makarova et al., 2012) emphasizing its tight relationship with normal DNA replication. Inhibition of REV3 expression in human cells leads to accumulation of DNA double strand breaks (DSB), activation of DNA damage response (DDR) and a reduced fraction of S-phase cells (Knobel et al., 2011), which results in increased formation of anaphase bridges and chromosomal breaks/gaps, expression of common fragile sites (CFS), genomic instability (Bhat et al., 2013) and ultimately cell cycle arrest or senescence (Knobel et al., 2011).

Cancer cells harbor multiple mutations in their genome, many of which affect DDR and lead to genomic instability but can be tolerated because of the redundant or complementary function of some of the DNA

repair pathways (Jackson and Bartek, 2009). Thus, targeting genes whose function becomes essential due to mutations in cancer cells is an attractive approach to cancer therapy (Kaelin, 2005). This so-called principle of synthetic sickness/lethality (SSL) demonstrated its applicability for targeted cancer therapy of BRCA2-deficient breast cancer by PARP-inhibitors not only at the bench (Bryant et al., 2005; Farmer et al., 2005) but also at the bedside (Fong et al., 2009). Recent publications follow this example by discovering synthetic lethality between MSH2 and DNA polymerase β (POLB), MLH1 and polymerase γ (POLG) (Martin et al., 2010) as well as Chk1 and polymerase λ (POLL) (Zucca et al., 2013), confirming that SSL between DDR genes is a common phenomenon.

Loss-of-function genetic screening is a powerful approach for novel target gene discovery that can be employed for detection of synthetic lethal gene interactions in cancer cells (reviewed in (Mullenders and Bernards, 2009; Nijman, 2011)). In particular, RNA interference technology was successfully used to identify vulnerabilities of cancers driven by certain oncogenes (Luo et al., 2009). Here, we took advantage of a whole human genome siRNA library to explore in an unbiased manner SSL in REV3-deficient cancer cells, in order to gain insight into cellular functions of REV3.

2. Material and methods

2.1. Cell culture, plasmid transfections, gene expression analysis

The non-small cell lung cancer (NSCLC) cell line A549 was authenticated by DNA fingerprinting of short tandem repeat loci (Microsynth, Switzerland). Stable cell lines used for the siRNA screening were generated by transfection of A549 cells with either the scrambled short hairpin RNA (shRNA) expressing plasmid shSCR or the REV3-silencing shRNA expression plasmid shREV3-4 (Knobel et al., 2011). Plasmid transfections were performed using Lipofectamine™ 2000 (Invitrogen) according to the manufacturer's instructions. Subsequent selection of resistant clones was performed with 1ug/ml puromycin. Gene knockdown was assessed by quantitative real-time PCR (rtPCR) measuring ΔΔCt values of the target gene versus control Histone H3 as described previously (Knobel et al., 2011). All cell lines were cultured in Dulbecco's Modified Eagle's Medium (DMEM) high glucose (Sigma) supplemented with 2 mM L-glutamine, 10% fetal calf serum (FCS) and 1% (w/v) penicillin/streptomycin. Cells were grown at 37°C in a humidified atmosphere containing 5% CO_2.

2.2. Reagents

For siRNA transfections, we used DharmaFECT 1 (DF) transfection reagent and siRNA duplexes acquired from Dharmacon (Thermo Fisher Scientific, USA). In the screen and the follow-up experiments, siGENOME non-targeting control pool#2 and the PLK1 SMARTpool siRNA were used as negative and positive control, respectively. For flow cytometry, immunoblotting and colony formation experiments, REV3 expression was silenced with ON-TARGETplus SMART pool REV3L (siREV3), while ON-TARGETplus non-targeting pool (siNT) was used as a negative control and buffer only treatment (buffer) was used to determine the effect of the transfection reagent.

Hydroxyurea (HU) was acquired from Applichem, Germany. CellTiter-Blue® Cell Viability Assay reagent was purchased from Promega, USA.

Oligonucleotides used for cloning and primers for rtPCR were ordered from Microsynth, Switzerland. Sequences of the rtPCR primers for REV3 and Histone H3 mRNA were disclosed previously (Knobel et al., 2011). The following primers were used for detection of RRM1 mRNA levels by qPCR: forward 5'-CCTGGGAACCATCAAATGCAGCAA-3' and reverse 5'- GGGCCAGGGAAGCCAAATTACAAA-3'.

2.3. Vector cloning and transfection

shREV3-4 and shSCR were introduced previously (Knobel et al., 2011). The short hairpin RRM1 oligos: 5'-GATCCCCGCACAGAAATAGTGGAGTATTCAAGAGATACTCCACTATTTCTGTGCTTTTTA-3' and 5'-AGCTTAAAAAGCACAGAAATAGTGGAGTATCTCTTGAATACTCCACTATTTCTGTGCGGG-3' were annealed and ligated into pSuperior.puro as described by the manufacturer (OligoEngine, Seattle, WA). The shRNA and H1 promoter fragments were subsequently transferred into the constitutive expressing lentiviral vector pLVTHM (Addgene, Cambridge, MA). Replication-deficient lentiviral particles were produced and titrated as described previously (Knobel et al., 2011)

2.4. Lentiviral transduction and colony formation assay

Lentiviral transduction and subsequent colony formation assay were performed as described previously (Knobel et al., 2011). For combined siRNA transfection, lentiviral transduction and subsequent colony formation, the procedure was as follows; 25,000 cells per well were seeded in 6-well plates and transfected 24 hours later with 50 nM siRNA (targeting REV3 or non-targeting control) using 80-times diluted DF. The medium was exchanged 24 hours after transfection. Another 24 hours later, cells were trypsinized, counted and 500 cells per well were seeded in 6-well plates for shRRM1 lentiviral transduction and colony formation assay, which was performed as described previously (Knobel et al., 2011).

2.5. Genome-wide siRNA screening and follow –up experiments

High-throughput screening (HTS) was done essentially as described previously (Siebring-van Olst et al., 2013). One day before siRNA transfection, S1C6 or R1B6 cells (750 cells per well) were seeded in 272 transparent flat-bottom 96-well plates (TPP, Switzerland) in 80 µl of complete culture medium. The next day, 10 µl of DF diluted 250-fold in DMEM was dispensed into 384-well siRNA library plates comprising the siARRAY human genome library and negative and positive control siRNAs at 2.5 pmol in 10 µl siRNA buffer (Dharmacon) prepared in advance. The resulting 20 µl transfection mixes were transferred to the cell culture plates, resulting in a final siRNA concentration of 25 nM. After transfection, cells were grown for 5 days before adding 20 µl per well CellTiter-Blue Reagent. The plates were incubated for 4 hours at 37°C following which 50 µl of 3% SDS solution was added to stop the reaction. Fluorescence was measured at 540 nm excitation and 590 nm emission wavelengths.

For the deconvolution of the siRNA pools, the experimental conditions were identical, i.e. 25 nM of siRNA and 0.04 µl of DF per well in 96-well plates. For double transfections, 25 nM of each siRNA and 0.08 µl of DF were used.

2.6. Data and statistical analysis

For reading, pre-processing and normalization of the raw fluorescence data, the *cellHTS2* Bioconductor package was employed (Boutros et al., 2006). The data were per plate normalized to the negative control and log-transformed. To generate the differential viability list, genes were sorted by the absolute difference of the mean viability scores for the two cell lines, each screened in two independent screens. Bayesian statistics for linear models in *limma* package (Smyth, 2004) was used to calculate the P-value for each gene. For gene set enrichment analysis we employed ROMER from *limma* (Majewski et al., 2010).

To assess statistical significance of treatment effects (siREV3, shREV3, shRRM1 and HU) and their interactions, two-way Analysis of Variance (ANOVA) was performed. The effect of siRNA transfection was inferred from the comparison of buffer only and siNT treated samples. To isolate the effects associated with silencing REV3 expression (iREV3) from the total effect of siREV3 transfection (siREV3) we presented the latter as a combination of pure silencing (iREV3) and other transfection effects that can be estimated from the effects of control non-targeting siRNA transfection (siNT). Both REV3 silencing

(iREV3) and control siRNA transfection (siNT) effects were assigned to the samples subjected to siREV3 transfection, thereby allowing estimation of the pure effect of REV3 silencing (iREV3). Following established methodology (Slinker, 1998), p-values of ANOVA interaction effects (e.g. HU:iREV3) were used as criteria for the statistical significance of treatments synergy. For pairwise comparisons, two-tailed Student's t test was employed.

2.7. Flow cytometry

For flow cytometry 25,000 cells per well were seeded in 6-well plates and transfected as described above (50 nM siRNA and 80-fold diluted DF). 24 hours after transfection, the medium was exchanged and another 24 hours later, cells were treated with 0.25 μM HU. After 24 hours, cells were labeled with 10 μM 5-ethynyl-2′-deoxyuridine (EdU) for 60 min (according to the manufacturer's instructions (C35002; Invitrogen)), harvested by trypsinization, and fixed for 20 min with ice-cold 70% Ethanol at room temperature. Cells were washed with 1% BSA/PBS, pH 7.4, permeabilized with 0.5% saponin/1% BSA/PBS for 10 minutes, and stained in the fixation buffer with anti–γH2AX antibody (05-636, EMD Millipore) or anti-RPA32/RPA2 antibody (ab2175, Abcam) overnight at 4°C, followed by incubation with a secondary antibody (a31553, Invitrogen) for 30 min at room temperature. Subsequently, cells were treated with 20ug/ml RNase A and DNA was stained with 0.5 μg/ml propidium iodide (Sigma-Aldrich). Cell fluorescence was measured on an Attune flow cytometer (Applied Biosystems) and analyzed with the Attune cytometric software v1.2.5 (Applied Biosystems). Buffer treated controls were used to set the gating threshold for γH2AX (and RPA) to 1% as described before (Kataoka et al., 2006).

2.8. Immunoblotting

Immunoblotting was performed essentially as described earlier (Knobel et al., 2011). The following primary antibodies were used: ATM-pS1981 (Epitomics, 2152-1, 1:1000), ATM (GeneTex GTX70103, 1:1000), Chk1-pS345 (Cell Signaling, 2348, 1:1000), Chk1 (Santa Cruz, sc-8408, 1:100).

3. Results

3.1. Generation and characterization of an isogenic pair of cell lines for REV3 synthetic sickness/lethality (SSL) screening

In order to define synthetic lethal gene interactions with REV3, we generated A549 NSCLC cell lines expressing short hairpin RNAs targeting REV3 and control cell lines expressing a shRNA with scrambled sequence. Multiple independent clones were made and tested. Translesion synthesis is a major pathway involved in bypass and repair of DNA crosslinks and it is known that reduction of REV3 levels is associated with increased sensitivity to DNA crosslinking agents (Enoiu et al., 2012; Hicks et al., 2010).Therefore, we based selection of the most suitable cell lines for screening on their REV3 expression levels and their cisplatin sensitivity as a functional readout.Two cell lines R1B6 and S1C6, ,expressing REV3 shRNA and a scrambled shRNA respectively, were selected for use in HTS. Compared to the parental cell line A549, the REV3 mRNA expression level in S1C6 cells was identical, whereas REV3 expression in R1B6 cells was decreased to 49% (Fig.1*A*). The cisplatin sensitivity assessed by quantitation of cell viability 5 days after continuous drug treatment, differed significantly for the two cell lines. The REV3 deficient cell line R1B6 was up to 2.7 times more sensitive than its proficient counterpart S1C6 (43% versus 16% at 3 μM, t-test $p<0.01$; Fig. 1*B*), indicating that the decrease of REV3 mRNA expression in R1B6 cells has functional consequence.

3.2. Genome-wide siRNA screening for REV3 SSL interactions

First, we optimized the HTS setup, with respect to number of seeded cells per well, suitable conditions for automated forward siRNA transfection and incubation time after transfection before assessing cell viability. The optimized transfection conditions resulted in efficient gene knockdown (Fig. A. 1) and were used for primary HTS and secondary confirmation experiments.

Next, whole human genome siRNA library screens were carried out with the pair of REV3 knockdown and control cell lines and cell viability as readout (Fig. 2). In detail, R1B6 or S1C6 cells were seeded in 96-well plates and transfected with the arrayed library comprising pooled siRNAs (4 siRNA per gene) targeting more than 20,000 human transcripts. The number of viable cells was assessed using CellTiter-Blue Cell Viability Assay and resulting values were normalized to non-targeting siRNA (siNT) controls included on every plate, log-transformed and scored. Both cell lines were screened twice. The screens showed high correlation between replicates, i.e. Pearson correlation coefficients between replicates was 0.87 for S1C6 and 0.84 for R1B6 (Table A. 1). Assay quality metrics were excellent, with Z' factors (Zhang et al., 1999) for positive (siPLK1) versus negative (siNT) controls generally exceeding 0.5. To identify genes whose silencing induced SSL specifically in REV3–deficient cells, the gene list with the corresponding values of viability was sorted by the absolute difference of the mean viability robust scores between S1C6 and R1B6 (Dataset B. 1). Genes were considered as primary hits when satisfied one of the following criteria: a differential viability score > 2.0 and $p<0.05$ (genes with the strongest differential effect, Table 1) or $p<5e-4$ and differential viability score > 0.8 (high confidence genes, Table 2). Table 1 gives the 9 genes that were selected this way and two additional genes - UBE2N and RRM2. UBE2N, which ranked 30 in the screen, was included in the Table 1 and the further analysis based on its known connection to TLS. UBE2N is the human homologue of UBC13 that is required for PCNA polyubiquitination promoting REV3-independent post-replication DNA repair in yeast (Ball et al., 2009).

Subsequently, selected primary screen hits were stratified by performing confirmation screens using S1C6 and R1B6 cells and the parental A549 lung cancer cells. First, we performed a secondary confirmation screen testing the siRNA pools used in the primary screens (Fig. 3*A*). Positive control siPLK1 included in this experiment exhibited a similar killing effect on the three cell lines, with residual viability in the range of 10-15%, indicating that transfection and knockdown was effective in all three cell lines. The REV3-deficient cell line R1B6 was more sensitive to silencing of the tested genes than the two control cell lines, confirming the validity of the results obtained by the high throughput screen. Next, we retested some of the genes by separately transfecting the 4 individual siRNAs targeting these genes. Fig. A. 2 represents the data for 10 selected genes (RRM1, LMTK3, CACNA1A, COPZ1, TXN, A1BG, KPNB1, CFLAR, GPR27 and UBE2N) that showed a synthetic lethal/proliferation defect phenotype with REV3 silencing in A549 NSCLC cells, confirmed in multiple independent experiments using 2 or more different siRNAs.

Silencing of RRM1, the large subunit of ribonucleotide reductase (RNR), showed the second strongest differential effect in the primary screen and a very robust profile in the deconvolution analysis, i.e. all four tested siRNAs had a more pronounced cytotoxic effect on REV3-deficient cells (Fig. A. 2). To validate this finding, and to exclude that the observed SSL was due to a clonal effect in R1B6 cells, we silenced REV3 with siRNA and RRM1 using a lentiviral vector expressing a short hairpin RNA (LV-shRRM1) in the parental A549 cells. Cell survival and proliferation capacity was measured by colony formation assay. Fig. 3*B* shows that siREV3 transfection in combination with lentiviral RRM1 silencing synergistically reduced colony formation (ANOVA, siREV3:LVshRRM1 $p=0.024$, Table A. 2).

3.3. Silencing REV3 in combination with inhibition of nucleotide synthesis synergistically reduces cancer cell growth.

RRM1 encodes the large subunit of ribonucleotide reductase (RNR). Notably, silencing of the small subunit of RNR, RRM2, also scored in the top 2% (rank 292). This suggests that inhibition of the catalytic function of RNR, rather than a subunit-specific effect, is involved in the observed reduction of the number

of cells in a REV3-deficient background. To corroborate this, we investigated if we could reproduce the REV3 SSL with a drug that inhibits RNR catalytic activity. Hydroxyurea (HU) is a drug used in the treatment of myeloproliferative disorders that inhibits RNR by scavenging tyrosyl free radicals of the small subunit required for reduction of ribonucleotides to deoxyribonucleotides. We performed colony formation assays after lentiviral transduction (with LV-shSCR or LV-shREV3) followed by continuous HU treatment (Fig. 4). To account for the effect of lentiviral transduction we included it in the ANOVA model for both LV-shSCR and LV-shREV3 transduced samples allowing calculation of the pure REV3 silencing effect (iREV3). While the colony formation was reduced by REV3 silencing alone (p=2.3e-13), its combination with HU treatment caused a more pronounced decrease in the number of cells than could be expected by mere superposition of the individual effects, the interaction effect (HU:iREV3) being statistically significant (ANOVA, p=0.018, Table A. 2).

RNR is a critical enzyme in *de novo* nucleotide synthesis. To assess whether alterations in nucleotide synthesis pathways in general are synergistic with REV3 silencing, we employed gene set enrichment analysis for linear models using rotation tests (ROMER) (Majewski et al., 2010), which is particularly suitable for the analysis of experiments with a small number of replicates (Dorum et al., 2009). We tested a set of KEGG pathways related to nucleotide metabolism (Table A. 3) and found that both purine and pyrimidine metabolisms were significantly enriched among the synthetic lethal genes (p-values 0.0041 and <1E-5, respectively). Since inhibition of RNR reduces the concentration of deoxyribonucleotides and leads to induction of replication stress (Feng et al., 2011), we tested whether the reduction in viability upon silencing of REV3 in combination with RNR inhibition can be extended to genes associated with replication stress. To guarantee an unbiased analysis, we generated a gene set by search of the NCBI human gene database with the term “replication stress” (Table A. 4). The replication stress gene set was also significantly enriched among the genes that had a high differential score in the screen (p=0.00034).

3.4. Down-regulation of REV3 expression enhances ssDNA formation induced by inhibition of ribonucleotide reductase

The SSL interaction of REV3-depletion with inhibition of the catalytic function of RNR and with silencing of genes associated with replication stress led us to hypothesize that REV3 might be involved in coping with nucleotide deprivation-induced replication stress in cancer cells. To test this hypothesis, we performed a series of flow cytometry experiments to investigate DNA synthesis, cell cycle distribution, DNA damage response and replication stress in A549 cells after REV3 silencing and HU treatment. The gating strategy for the flow cytometry experiments is illustrated in Fig. A. 3.

HU treatment inhibited DNA synthesis, as evidenced by a reduced median EdU incorporation (Fig. 5*A*). Silencing of REV3 significantly enhanced DNA synthesis inhibition by HU (siREV3 transfection and HU treatment compared to siNT transfection and HU treatment; t-test p<0.05). RPA2 is a subunit of replication protein A (RPA), a protein that binds single-stranded DNA (ssDNA). Detection of chromatin-bound RPA can be used to track the increase in cellular ssDNA (Forment et al., 2012), a characteristic feature of replication stress (Vassin et al., 2009). Down-regulation of REV3 expression did not change significantly the fraction of RPA2-positive cells, compared to siNT control transfection (Fig. 5*B*). In contrast, HU treatment significantly increased the number of RPA2-positive cells. Both control and REV3 siRNA transfections augmented the increase in ssDNA in response to HU, but this effect was stronger upon REV3 silencing. The synergy between HU treatment and REV3 silencing was significant evidenced by the p-value for the interaction effect HU:iREV3 (ANOVA, p=0.048, Table A. 2). An increased RPA2 signal can not only be due to enhanced replication stress but also to increased DNA end-resection during the process of DSB repair. To differentiate between these two possible causes we investigated whether the observed increase in RPA staining was accompanied by changes in DNA damage response. Phosphorylated histone H2AX (γH2AX) is a marker for the cellular response to various types of DNA damage including DSBs (Marti et al., 2006). HU treatment was associated with a moderate but significant

increase in the fraction of γH2AX positive cells (Fig 5C). Unexpectedly, siNT transfection increased γH2AX induction by HU treatment (ANOVA, HU:siNT p=0.016, Table A. 2), whereas siREV3 transfection did not lead to a significant change compared to HU-only treated cells (t-test, HU vs HU+siREV3 NS). Interestingly, comparison of siNT+HU and siREV3+HU revealed a significant decrease of H2AX phosphorylation after REV3 silencing and subsequent HU treatment (ANOVA, HU:iREV3 p=8.8e-4, Table A. 2). Hence, REV3 silencing did not promote DSB induction in response to HU treatment. In fact, it seemed to inhibit HU-induced DNA damage accumulation as demonstrated by decreased H2AX phosphorylation. Nevertheless, this observation has to be interpreted with a certain caution due to the strong effect of the control transfection.

To further investigate in more detail the role of REV3 in counteracting replication stress, we analyzed the cell cycle distribution after inhibition of REV3 expression and HU treatment (Fig. 6 *A-C*). In the absence of HU treatment, REV3 silencing significantly decreased the fraction of cells in S-phase, whereas the fraction of cells in the G_2-phase of the cell cycle was significantly increased, confirming an earlier observation (Knobel et al., 2011). This is in agreement with a suggested function of REV3 outside of S-phase (Brondello et al., 2008). As expected, HU treatment induced a pronounced S-phase accumulation. This accumulation was not further enhanced by additional REV3 silencing, but notably also REV3-specific S-phase depletion was not detected. Combination of HU treatment and REV3 silencing lead to a significant synergistic increase in S- and decrease in G_2 cell fractions (ANOVA, HU:iREV3 p=0.0062 and 3.9e-5 respectively, Table A. 2) reflecting that HU treatment perturbed the cell cycle distribution of REV3-deficient cells more than that of controls. Thus, the increase in the fraction of S-phase cells induced by HU treatment was more pronounced in REV3-deficient compared to REV3-proficient cells suggesting an increased role of REV3 in S-phase cells upon HU treatment. We observed that the fraction of sub-G_1 cells did not change upon HU treatment alone (3.5±0.4%, P=0.54) and combined REV3 silencing and HU treatment (3.3±1.4%, P=0.50) compared to control (4.2±1.7%) implying that observed synergy is rather due to proliferation defect than induction of apoptosis. We also compared the fractions of RPA positive cells in different cell cycle phases (Fig.6 *D-F*). The S-phase fraction of siREV3+HU treated cells contained a significantly larger proportion of RPA positive cells than the S-phase fractions of siNT+HU or HU treated cells (t-test, $p<0.05$). Such a difference was not observed in G_1- and G_2-phases. This indicates that the synergistic increase in cellular ssDNA upon combined siREV3 transfection and HU treatment (see Fig. 5) occurs mainly in the S-phase of the cell cycle. This is consistent with the role of polζ in DNA replication upon RS.

3.5. REV3 silencing enhances RS signaling

To investigate whether increased H2AX phosphorylation is due to RS-induced DSB formation, we performed immunoblotting analysis of ATM phosphorylation. ATM phosphorylation at serine 1981 is a specific marker for DSBs (So et al., 2009). In addition, CHK1 is phosphorylated by ATR in response to replication fork stalling and was used to assess the quantity of stalled but not resolved or collapsed replication forks. HU treatment solely induced CHK1 phosphorylation whereas ionizing radiation, as a positive control for DSBs, mainly induced ATM phosphorylation (Fig. 7). Treatment with 2 mM HU for 80 minutes resulted in phosphorylation of both CHK1 and ATM. Immunoblotting analysis revealed that the response to HU treatment was affected by both preceding siNT and siREV3 transfections. In detail, preceding control transfection increased HU-induced p-ATM and decreased p-CHK1, which might be attributable to collapsed replication forks due to the increased effective HU concentration upon transfection, as discussed below. In comparison, HU treatment after siREV3 transfection leads only to a modest increase in ATM phosphorylation but further enhances CHK1 phosphorylation, which might indicate accumulation of stalled but intact replication forks.

4. Discussion

This study aimed to identify SSL gene interactions with REV3 in lung cancer cells. For screening, we used stable cell lines obtained from A549 NSCLC cells carrying a plasmid vector expressing a short hairpin against REV3 or a scrambled control shRNA. The approximately 50% decrease in REV3 mRNA expression in the cell line R1B6 is of physiological relevance since it conferred cisplatin sensitivity.

Screening with a whole human genome siRNA library allowed us to determine synthetic lethal interactions with REV3 in an unbiased way. Statistically significant hits were ranked according to their differential inhibition of cell viability in the pair of cell lines. Consequently, a top position of a gene in the primary hit list indicates that the proliferation of the NSCLC cells is heavily dependent on this gene in a REV3-deficiency dependent manner. Our analysis revealed that silencing of RRM1, the large subunit of RNR, had the second most pronounced effect in reduction of cell viability specifically in a REV3-deficient background. Additionally, RRM2, the small subunit of RNR, also ranked among the top 2% genes in our screen, further corroborating that inhibition of RNR is synthetic lethal with REV3 depletion. RRM2 is overexpressed in many tumor types. For example, it was shown that RRM2 is highly (~15x) overexpressed in NSCLC (Hou et al., 2010). Moreover, RRM2 was suggested to act in cooperation with a variety of oncogenes to increase their transformation and tumorigenic potential (Fan et al., 1998). It is well known that inhibition of RNR function affects proliferation of cancer cells to a greater extent than normal cells, which allows successful application of small molecule inhibitors targeting RNR in the clinic for cancer treatment (reviewed in (Cerqueira et al., 2005)). Together, these data suggest that cancer cells are frequently addicted to RNR overexpression. Therefore, we further focused our analysis on the synthetic lethal interaction of REV3 with RNR.

Downregulation of RRM1 expression and treatment with HU, a drug inhibiting small subunit RRM2 of RNR, in combination with transient siRNA-based depletion of REV3 resulted in synergistic inhibition of cell proliferation (i.e. synthetic sickness or proliferation defect) as indicated by reduced EdU incorporation. This indicates that the observed effects are not RNR-subunit specific but rather related to RNR catalytic function. Inhibition of RNR catalytic activity leads to deprivation of deoxyribonucleotides, reduced replication rate and stalling of replication forks (Petermann et al., 2010). Higher concentrations of HU (~2mM) can induce complete cell cycle arrest, which is often exploited for synchronization of cultured cells. The concentrations that we used (0.2-0.3 mM) show very limited cytotoxicity and allow replication sufficient for colony formation experiments even upon long–term treatment (Fig. 3). In addition, the absence of a significant increase in sub-G_1 cell fraction upon HU and HU+siREV3 treatments indicates that 24 hours treatment with these HU concentrations does not induce apoptosis. However these concentrations are sufficient to create nucleotide pool imbalance (Skog et al., 1992), thereby generating conditions of mild replication stress. Therefore, we tested whether RS-related genes were overrepresented among the genes whose silencing induced SSL in the REV3-deficient background and found this enrichment to be significant.

We proceeded with detection of chromatin-bound RPA, an indicator for replication-associated ssDNA formation, and controlling levels of DNA damage measured by H2AX phosphorylation. Compared to individual treatments, combination of HU treatment with REV3 silencing synergistically increased the fraction of RPA positive cells, which was not accompanied by increased levels of γH2AX. Thus, under conditions of HU-induced RS, silencing of REV3 in the lung cancer cell line A549 impairs DNA replication but does not lead to increased DNA damage accumulation, indicating that polζ is directly involved in DNA replication. This is further corroborated by our finding that the fraction of S-phase cells after siREV3+HU treatment is significantly higher than could be expected from a simple additive effect of HU treatment and REV3 silencing, which suggests an important role of REV3 in the DNA synthesis of HU-treated cells. Moreover, the significant increase in RPA positive cells upon combined HU treatment and REV3 silencing

(HU+siREV3 vs HU+siNT) was found only in S phase and not in G_1 and G_2 phases of the cell cycle, whereas both G_2 and S phases would be affected if homologous recombination was involved.

We did not expect that the concentrations of HU that we used would strongly induce DNA damage since treatment of human cancer cells with 8 times higher HU concentration for the same time (24 hours) resulted only in a moderate induction of DSBs as shown by pulse-field gel electrophoresis (Petermann et al., 2010). Also single stranded breaks were not detected by alkaline unwinding technique (Skog et al., 1992) after treatment with a comparably low concentration of HU (0.1 mM). Nevertheless, due to the high sensitivity of the flow cytometry method, we detected increased H2AX phosphorylation upon HU treatment that was further increased by preceding transfection with control siRNA. Lipid-mediated siRNA transfection is known to affect permeability of the cell membrane. In analogy, we speculate that the increased γH2AX and RPA2 signals detectable after control transfection and subsequent HU treatment might be explained by the increased drug penetration and therefore a higher effective intracellular HU concentration even when cells were treated after removal of the transfection reagent.

It was previously reported that DNA damage induced H2AX phosphorylation is replication dependent and can be reduced by contact inhibition (Marti et al., 2006). Our analysis of EdU incorporation revealed that HU treatment significantly reduced the fraction of replicating cells in REV3-deficient cells compared to REV3-proficient cells. Thus, we speculate that the reduced level of γH2AX (by flow cytometry) and the diminished ATM phosphorylation (by immunoblotting analysis) in siREV3+HU treated cells compared to siNT+HU control cells might be attributed to the decreased DNA replication rate upon REV3 silencing and subsequent reduction of HU-induced replication fork breakage. Similarly, replication slowdown upon REV3 silencing and subsequent HU treatment might also explain the reduced rate of replication-associated fork collapse., However, due to strong influence of siNT transfection on cells, these data should be regarded as inconclusive. Consequently, it is a matter of further investigations to elucidate in more detail whether REV3 silencing inhibits replication fork collapse upon RS.

Nucleotide concentrations are tightly regulated throughout the cell cycle and perturbation of this regulation leads to increased mutation rate (Kumar et al., 2011). One of the key components of this regulation is the regulation of RNR activity. In yeast, upregulation of RNR activity increases replication fork speed, indicating that nucleotide pools are limiting for normal DNA replication (Poli et al., 2012). Both in yeast and mammalian cells, nucleotide pools are expanded upon entry in the S-phase. In mammalian cells, exit from S phase is associated with a decrease of dNTP pools, most notably of dCTP changing 3-fold (Leeds et al., 1985; Skoog et al., 1973). The absolute changes of nuclear nucleotide pools during the cell cycle are even more pronounced (Bjursell and Skoog, 1980) perhaps making them limiting for late DNA replication. Thus, in addition to the role of Polζ in replication after HU-generated nucleotide deprivation, we speculate that Polζ might also be involved in the late DNA replication. In this context, the recently discovered role of Polζ in the stability of fragile sites (Bhat et al., 2013) can be viewed as a particular case of late DNA replication, since fragile sites are known to be replicated late during the cell cycle and their stability is compromised by RS inducing agents (aphidicolin, hydroxyurea, low folate medium). In detail, common fragile sites (CFS) are replicated in late S phase and their replication is even further delayed by aphidicolin, causing the replication of CFS to persist in G_2 phase (Le Beau et al., 1998). In our study, upon REV3 silencing in the absence of HU treatment, an increase in the fraction of cells in the G_2-phase was the most prominent effect (1.5 fold), suggesting that REV3 plays its most important role in this cell cycle phase, which is in agreement with the recently reported enrichment of REV3 on the chromatin in G_2/M and its role in fragile site maintenance (Bhat et al., 2013). However, HU treatment increased the S-phase fraction of REV3 depleted cells more than that of cells without REV3 silencing, which suggests that REV3 has increased importance in S-phase upon HU treatment. Thus, we speculate that under our experimental conditions, the HU treatment induces in A549 cells the early onset of the “late DNA replication”, which typically occurs during G_2-phase, already in S-phase by creating conditions of nucleotide shortage. In other words, REV3

function in replication does not seem to be confined to a certain cell cycle phase but it rather becomes important whenever replication problems are encountered.

Late replicating DNA regions were previously shown to be particularly prone to mutagenesis in both yeast (Agier and Fischer, 2012) and humans (Stamatoyannopoulos et al., 2009), indicating a likely conservation of the mechanism underlying this phenomenon. In yeast, comparison of available catalytic K_m parameters of polymerases ζ, δ and η (Table A. 5) suggests that in the conditions of nucleotide shortage ($dN<<K_m$) Polζ can bind nucleotides with the highest affinity, because its K_m values for incorporation of 3 nucleotides are 5-20 times lower than those of Polδ. This is due to Polζ lysine residue K1061 that binds the triphosphate group of nucleotides, increasing the binding affinity, but decreasing replication fidelity (Howell et al., 2008; Zhong et al., 2006). This error-prone nature of Polζ suggests that it can contribute to the late replication mutagenesis by participating in this process as suggested above.

Nucleotide biosynthesis is commonly upregulated in cancer cells to cope with their increased metabolic requirements (Tong et al., 2009). Therefore, many oncogenes not only induce replication stress (Gorgoulis et al., 2005) (Halazonetis et al., 2008; Neelsen et al., 2013), but also activate nucleotide synthesis (Bester et al., 2011). Consequently, concentrations of the 4 dNTPs in tumor cells are on average 6-11 fold higher than in normal cells (Traut, 1994). But, if a cancer cell fails to adjust its metabolism, nucleotide deficiency promotes genomic instability (Bester et al., 2011) and also can lead to oncogene-induced senescence (Aird et al., 2013). Interestingly, cells lacking REV3 undergo senescence and accumulate persistent DNA DSBs at later time points (Knobel et al., 2011; Lange et al., 2013), possibly reflecting their inability to cope with RS (Feng et al., 2011). Based on our present findings it is tempting to hypothesize that oncogene-induced RS could be the unifying feature responsible for the observed cancer cell specific growth arrest upon REV3 silencing described earlier by our group (Knobel et al., 2011).

The function of Polζ in DNA replication under conditions of nucleotide deficiency-associated replication stress might also help in understanding its role in embryogenesis. Rev3 knockout is embryonic lethal in mice causing depletion of the hematopoietic compartment and embryonic stem cells (Esposito et al., 2000). A recent study showed that hematopoietic tissue is highly prone to RS associated with nucleotide pool imbalance (Austin et al., 2012). Besides, human embryonic stem cells are very sensitive to RS (Desmarais et al., 2012) and high levels of RS are observed upon stem cell induction (Pasi et al., 2011). Apparently, hematopoietic and embryonic stem cells overexpress REV3 in order to cope with excessive RS and suffer the most from REV3 depletion.

In summary, our study identifies a novel function of human polζ in coping with replication stress thereby broadening our understanding of its role in cell biology.

Appendices A and B. Supplementary material

Supplementary figures and tables (Appendix A) and Dataset B. 1 (Appendix B) are available online, including Supplementary References (Dieckman et al., 2010; Haracska et al., 2001; Johnson et al., 2003; Washington et al., 1999).

Conflict of interest

The authors declare no conflict of interest.

Acknowledgements

We thank Renee X. de Menezes for R scripts and help in statistical analysis of the data. This work was supported by the Walter Bruckerhoff Stiftung and by the Stichting VUmc CCA.

REFERENCES

Agier, N., Fischer, G., 2012. The mutational profile of the yeast genome is shaped by replication. Mol Biol Evol 29, 905-913.

Aird, K.M., Zhang, G., Li, H., Tu, Z., Bitler, B.G., Garipov, A., Wu, H., Wei, Z., Wagner, S.N., Herlyn, M., Zhang, R., 2013. Suppression of nucleotide metabolism underlies the establishment and maintenance of oncogene-induced senescence. Cell Rep 3, 1252-1265.

Austin, W.R., Armijo, A.L., Campbell, D.O., Singh, A.S., Hsieh, T., Nathanson, D., Herschman, H.R., Phelps, M.E., Witte, O.N., Czernin, J., Radu, C.G., 2012. Nucleoside salvage pathway kinases regulate hematopoiesis by linking nucleotide metabolism with replication stress. J Exp Med 209, 2215-2228.

Ball, L.G., Zhang, K., Cobb, J.A., Boone, C., Xiao, W., 2009. The yeast Shu complex couples error-free post-replication repair to homologous recombination. Molecular microbiology 73, 89-102.

Bester, A.C., Roniger, M., Oren, Y.S., Im, M.M., Sarni, D., Chaoat, M., Bensimon, A., Zamir, G., Shewach, D.S., Kerem, B., 2011. Nucleotide deficiency promotes genomic instability in early stages of cancer development. Cell 145, 435-446.

Bhat, A., Andersen, P.L., Qin, Z., Xiao, W., 2013. Rev3, the catalytic subunit of Polzeta, is required for maintaining fragile site stability in human cells. Nucleic Acids Res 41, 2328-2339.

Bjursell, G., Skoog, L., 1980. Control of nucleotide pools in mammalian cells. Antibiotics and chemotherapy 28, 78-85.

Boutros, M., Bras, L.P., Huber, W., 2006. Analysis of cell-based RNAi screens. Genome Biol 7, R66.

Brondello, J.M., Pillaire, M.J., Rodriguez, C., Gourraud, P.A., Selves, J., Cazaux, C., Piette, J., 2008. Novel evidences for a tumor suppressor role of Rev3, the catalytic subunit of Pol zeta. Oncogene 27, 6093-6101.

Bryant, H.E., Schultz, N., Thomas, H.D., Parker, K.M., Flower, D., Lopez, E., Kyle, S., Meuth, M., Curtin, N.J., Helleday, T., 2005. Specific killing of BRCA2-deficient tumours with inhibitors of poly(ADP-ribose) polymerase. Nature 434, 913-917.

Cerqueira, N.M., Pereira, S., Fernandes, P.A., Ramos, M.J., 2005. Overview of ribonucleotide reductase inhibitors: an appealing target in anti-tumour therapy. Curr Med Chem 12, 1283-1294.

Covo, S., de Villartay, J.P., Jeggo, P.A., Livneh, Z., 2009. Translesion DNA synthesis-assisted non-homologous end-joining of complex double-strand breaks prevents loss of DNA sequences in mammalian cells. Nucleic Acids Res 37, 6737-6745.

Desmarais, J.A., Hoffmann, M.J., Bingham, G., Gagou, M.E., Meuth, M., Andrews, P.W., 2012. Human embryonic stem cells fail to activate CHK1 and commit to apoptosis in response to DNA replication stress. Stem Cells 30, 1385-1393.

Dieckman, L.M., Johnson, R.E., Prakash, S., Washington, M.T., 2010. Pre-steady state kinetic studies of the fidelity of nucleotide incorporation by yeast DNA polymerase delta. Biochemistry 49, 7344-7350.

Dorum, G., Snipen, L., Solheim, M., Saebo, S., 2009. Rotation testing in gene set enrichment analysis for small direct comparison experiments. Stat Appl Genet Mol Biol 8, Article34.

Enoiu, M., Jiricny, J., Scharer, O.D., 2012. Repair of cisplatin-induced DNA interstrand crosslinks by a replication-independent pathway involving transcription-coupled repair and translesion synthesis. Nucleic Acids Res 40, 8953-8964.

Esposito, G., Godindagger, I., Klein, U., Yaspo, M.L., Cumano, A., Rajewsky, K., 2000. Disruption of the Rev3l-encoded catalytic subunit of polymerase zeta in mice results in early embryonic lethality. Curr Biol 10, 1221-1224.

Fan, H., Villegas, C., Huang, A., Wright, J.A., 1998. The mammalian ribonucleotide reductase R2 component cooperates with a variety of oncogenes in mechanisms of cellular transformation. Cancer Res 58, 1650-1653.
Farmer, H., McCabe, N., Lord, C.J., Tutt, A.N., Johnson, D.A., Richardson, T.B., Santarosa, M., Dillon, K.J., Hickson, I., Knights, C., Martin, N.M., Jackson, S.P., Smith, G.C., Ashworth, A., 2005. Targeting the DNA repair defect in BRCA mutant cells as a therapeutic strategy. Nature 434, 917-921.
Feng, W., Di Rienzi, S.C., Raghuraman, M.K., Brewer, B.J., 2011. Replication stress-induced chromosome breakage is correlated with replication fork progression and is preceded by single-stranded DNA formation. G3 (Bethesda) 1, 327-335.
Fong, P.C., Boss, D.S., Yap, T.A., Tutt, A., Wu, P., Mergui-Roelvink, M., Mortimer, P., Swaisland, H., Lau, A., O'Connor, M.J., Ashworth, A., Carmichael, J., Kaye, S.B., Schellens, J.H., de Bono, J.S., 2009. Inhibition of poly(ADP-ribose) polymerase in tumors from BRCA mutation carriers. N Engl J Med 361, 123-134.
Forment, J.V., Walker, R.V., Jackson, S.P., 2012. A high-throughput, flow cytometry-based method to quantify DNA-end resection in mammalian cells. Cytometry. Part A : the journal of the International Society for Analytical Cytology 81, 922-928.
Gorgoulis, V.G., Vassiliou, L.V., Karakaidos, P., Zacharatos, P., Kotsinas, A., Liloglou, T., Venere, M., Ditullio, R.A., Jr., Kastrinakis, N.G., Levy, B., Kletsas, D., Yoneta, A., Herlyn, M., Kittas, C., Halazonetis, T.D., 2005. Activation of the DNA damage checkpoint and genomic instability in human precancerous lesions. Nature 434, 907-913.
Halazonetis, T.D., Gorgoulis, V.G., Bartek, J., 2008. An oncogene-induced DNA damage model for cancer development. Science 319, 1352-1355.
Haracska, L., Unk, I., Johnson, R.E., Johansson, E., Burgers, P.M., Prakash, S., Prakash, L., 2001. Roles of yeast DNA polymerases delta and zeta and of Rev1 in the bypass of abasic sites. Genes & development 15, 945-954.
Hicks, J.K., Chute, C.L., Paulsen, M.T., Ragland, R.L., Howlett, N.G., Gueranger, Q., Glover, T.W., Canman, C.E., 2010. Differential roles for DNA polymerases eta, zeta, and REV1 in lesion bypass of intrastrand versus interstrand DNA cross-links. Mol Cell Biol 30, 1217-1230.
Hou, J., Aerts, J., den Hamer, B., van Ijcken, W., den Bakker, M., Riegman, P., van der Leest, C., van der Spek, P., Foekens, J.A., Hoogsteden, H.C., Grosveld, F., Philipsen, S., 2010. Gene expression-based classification of non-small cell lung carcinomas and survival prediction. PloS one 5, e10312.
Howell, C.A., Kondratick, C.M., Washington, M.T., 2008. Substitution of a residue contacting the triphosphate moiety of the incoming nucleotide increases the fidelity of yeast DNA polymerase zeta. Nucleic Acids Res 36, 1731-1740.
Jackson, S.P., Bartek, J., 2009. The DNA-damage response in human biology and disease. Nature 461, 1071-1078.
Johnson, R.E., Prakash, L., Prakash, S., 2012. Pol31 and Pol32 subunits of yeast DNA polymerase delta are also essential subunits of DNA polymerase zeta. Proc Natl Acad Sci U S A 109, 12455-12460.
Johnson, R.E., Yu, S.L., Prakash, S., Prakash, L., 2003. Yeast DNA polymerase zeta (zeta) is essential for error-free replication past thymine glycol. Genes & development 17, 77-87.
Kaelin, W.G., Jr., 2005. The concept of synthetic lethality in the context of anticancer therapy. Nat Rev Cancer 5, 689-698.
Kataoka, Y., Bindokas, V.P., Duggan, R.C., Murley, J.S., Grdina, D.J., 2006. Flow cytometric analysis of phosphorylated histone H2AX following exposure to ionizing radiation in human microvascular endothelial cells. Journal of radiation research 47, 245-257.
Knobel, P.A., Kotov, I.N., Felley-Bosco, E., Stahel, R.A., Marti, T.M., 2011. Inhibition of REV3 expression induces persistent DNA damage and growth arrest in cancer cells. Neoplasia 13, 961-970.
Knobel, P.A., Marti, T.M., 2011. Translesion DNA synthesis in the context of cancer research. Cancer Cell Int 11, 39.

Kumar, D., Abdulovic, A.L., Viberg, J., Nilsson, A.K., Kunkel, T.A., Chabes, A., 2011. Mechanisms of mutagenesis in vivo due to imbalanced dNTP pools. Nucleic Acids Res 39, 1360-1371.
Lange, S.S., Bedford, E., Reh, S., Wittschieben, J.P., Carbajal, S., Kusewitt, D.F., DiGiovanni, J., Wood, R.D., 2013. Dual role for mammalian DNA polymerase zeta in maintaining genome stability and proliferative responses. Proc Natl Acad Sci U S A 110, E687-696.
Le Beau, M.M., Rassool, F.V., Neilly, M.E., Espinosa, R., 3rd, Glover, T.W., Smith, D.I., McKeithan, T.W., 1998. Replication of a common fragile site, FRA3B, occurs late in S phase and is delayed further upon induction: implications for the mechanism of fragile site induction. Hum Mol Genet 7, 755-761.
Leeds, J.M., Slabaugh, M.B., Mathews, C.K., 1985. DNA precursor pools and ribonucleotide reductase activity: distribution between the nucleus and cytoplasm of mammalian cells. Mol Cell Biol 5, 3443-3450.
Luo, J., Emanuele, M.J., Li, D., Creighton, C.J., Schlabach, M.R., Westbrook, T.F., Wong, K.K., Elledge, S.J., 2009. A genome-wide RNAi screen identifies multiple synthetic lethal interactions with the Ras oncogene. Cell 137, 835-848.
Majewski, I.J., Ritchie, M.E., Phipson, B., Corbin, J., Pakusch, M., Ebert, A., Busslinger, M., Koseki, H., Hu, Y., Smyth, G.K., Alexander, W.S., Hilton, D.J., Blewitt, M.E., 2010. Opposing roles of polycomb repressive complexes in hematopoietic stem and progenitor cells. Blood 116, 731-739.
Makarova, A.V., Stodola, J.L., Burgers, P.M., 2012. A four-subunit DNA polymerase zeta complex containing Pol delta accessory subunits is essential for PCNA-mediated mutagenesis. Nucleic Acids Res 40, 11618-11626.
Marti, T.M., Hefner, E., Feeney, L., Natale, V., Cleaver, J.E., 2006. H2AX phosphorylation within the G1 phase after UV irradiation depends on nucleotide excision repair and not DNA double-strand breaks. Proceedings of the National Academy of Sciences of the United States of America 103, 9891-9896.
Martin, S.A., McCabe, N., Mullarkey, M., Cummins, R., Burgess, D.J., Nakabeppu, Y., Oka, S., Kay, E., Lord, C.J., Ashworth, A., 2010. DNA polymerases as potential therapeutic targets for cancers deficient in the DNA mismatch repair proteins MSH2 or MLH1. Cancer Cell 17, 235-248.
Mullenders, J., Bernards, R., 2009. Loss-of-function genetic screens as a tool to improve the diagnosis and treatment of cancer. Oncogene 28, 4409-4420.
Neelsen, K.J., Zanini, I.M., Herrador, R., Lopes, M., 2013. Oncogenes induce genotoxic stress by mitotic processing of unusual replication intermediates. J Cell Biol 200, 699-708.
Nijman, S.M., 2011. Synthetic lethality: general principles, utility and detection using genetic screens in human cells. FEBS Lett 585, 1-6.
Northam, M.R., Robinson, H.A., Kochenova, O.V., Shcherbakova, P.V., 2010. Participation of DNA polymerase zeta in replication of undamaged DNA in Saccharomyces cerevisiae. Genetics 184, 27-42.
Pasi, C.E., Dereli-Oz, A., Negrini, S., Friedli, M., Fragola, G., Lombardo, A., Van Houwe, G., Naldini, L., Casola, S., Testa, G., Trono, D., Pelicci, P.G., Halazonetis, T.D., 2011. Genomic instability in induced stem cells. Cell Death Differ 18, 745-753.
Petermann, E., Orta, M.L., Issaeva, N., Schultz, N., Helleday, T., 2010. Hydroxyurea-stalled replication forks become progressively inactivated and require two different RAD51-mediated pathways for restart and repair. Mol Cell 37, 492-502.
Poli, J., Tsaponina, O., Crabbe, L., Keszthelyi, A., Pantesco, V., Chabes, A., Lengronne, A., Pasero, P., 2012. dNTP pools determine fork progression and origin usage under replication stress. EMBO J 31, 883-894.
Sharma, S., Hicks, J.K., Chute, C.L., Brennan, J.R., Ahn, J.Y., Glover, T.W., Canman, C.E., 2012. REV1 and polymerase zeta facilitate homologous recombination repair. Nucleic Acids Res 40, 682-691.
Siebring-van Olst, E., Vermeulen, C., de Menezes, R.X., Howell, M., Smit, E.F., van Beusechem, V.W., 2013. Affordable luciferase reporter assay for cell-based high-throughput screening. J Biomol Screen 18, 453-461.
Skog, S., Heiden, T., Eriksson, S., Wallstrom, B., Tribukait, B., 1992. Hydroxyurea-induced cell death in human T lymphoma cells as related to imbalance in DNA/protein cycle and deoxyribonucleotide pools and DNA strand breaks. Anticancer Drugs 3, 379-386.

Skoog, K.L., Nordenskjold, B.A., Bjursell, K.G., 1973. Deoxyribonucleoside-triphosphate pools and DNA synthesis in synchronized hamster cells. Eur J Biochem 33, 428-432.
Slinker, B.K., 1998. The statistics of synergism. Journal of molecular and cellular cardiology 30, 723-731.
Smyth, G.K., 2004. Linear models and empirical bayes methods for assessing differential expression in microarray experiments. Stat Appl Genet Mol Biol 3, Article3.
So, S., Davis, A.J., Chen, D.J., 2009. Autophosphorylation at serine 1981 stabilizes ATM at DNA damage sites. The Journal of cell biology 187, 977-990.
Stamatoyannopoulos, J.A., Adzhubei, I., Thurman, R.E., Kryukov, G.V., Mirkin, S.M., Sunyaev, S.R., 2009. Human mutation rate associated with DNA replication timing. Nat Genet 41, 393-395.
Tong, X., Zhao, F., Thompson, C.B., 2009. The molecular determinants of de novo nucleotide biosynthesis in cancer cells. Curr Opin Genet Dev 19, 32-37.
Traut, T.W., 1994. Physiological concentrations of purines and pyrimidines. Mol Cell Biochem 140, 1-22.
Vassin, V.M., Anantha, R.W., Sokolova, E., Kanner, S., Borowiec, J.A., 2009. Human RPA phosphorylation by ATR stimulates DNA synthesis and prevents ssDNA accumulation during DNA-replication stress. J Cell Sci 122, 4070-4080.
Washington, M.T., Johnson, R.E., Prakash, S., Prakash, L., 1999. Fidelity and processivity of Saccharomyces cerevisiae DNA polymerase eta. The Journal of biological chemistry 274, 36835-36838.
Wittschieben, J., Shivji, M.K., Lalani, E., Jacobs, M.A., Marini, F., Gearhart, P.J., Rosewell, I., Stamp, G., Wood, R.D., 2000. Disruption of the developmentally regulated Rev3l gene causes embryonic lethality. Curr Biol 10, 1217-1220.
Wittschieben, J.P., Patil, V., Glushets, V., Robinson, L.J., Kusewitt, D.F., Wood, R.D., 2010. Loss of DNA polymerase zeta enhances spontaneous tumorigenesis. Cancer Res 70, 2770-2778.
Zhang, J.H., Chung, T.D., Oldenburg, K.R., 1999. A Simple Statistical Parameter for Use in Evaluation and Validation of High Throughput Screening Assays. J Biomol Screen 4, 67-73.
Zhong, X., Garg, P., Stith, C.M., Nick McElhinny, S.A., Kissling, G.E., Burgers, P.M., Kunkel, T.A., 2006. The fidelity of DNA synthesis by yeast DNA polymerase zeta alone and with accessory proteins. Nucleic Acids Res 34, 4731-4742.
Zucca, E., Bertoletti, F., Wimmer, U., Ferrari, E., Mazzini, G., Khoronenkova, S., Grosse, N., van Loon, B., Dianov, G., Hubscher, U., Maga, G., 2013. Silencing of human DNA polymerase lambda causes replication stress and is synthetically lethal with an impaired S phase checkpoint. Nucleic Acids Res 41, 229-241.

Tables

Rank	Gene	P-value	Viability difference score	Gene name
1	GPR27	1.7E-03	2.67	G protein-coupled receptor 27
2	RRM1	1.6E-02	2.49	ribonucleotide reductase M1
3	CFLAR	4.9E-05	2.24	CASP8 and FADD-like apoptosis regulator
4	LMTK3	1.2E-02	2.19	lemur tyrosine kinase 3
5	CCR6	4.6E-04	2.13	chemokine (C-C motif) receptor 6
7	CACNA1A	2.3E-03	2.10	calcium channel, voltage-dependent, P/Q type, alpha 1A subunit
8	COPZ1	9.4E-03	2.09	coatomer protein complex, subunit zeta 1
9	CDY1	2.4E-02	2.09	chromodomain protein, Y-linked, 1
10	CSAD	2.2E-02	2.08	cysteine sulfinic acid decarboxylase
…	…	…	…	…
30	UBE2N	8.4E-04	1.63	ubiquitin-conjugating enzyme E2N (UBC13 homolog)
292	RRM2	4.9E-03	0.85	ribonucleotide reductase M2

Table 1. Highest ranking genes with a stronger effect on viability of REV3-deficient cells compared to control cells. All the genes in the screen were scored based on the normalized viability of the cells after silencing. Genes are ranked according to the difference of scores for control and REV3-deficient cell lines. A filter of P<0.05 is applied to exclude low-confidence genes. Results are from four whole-genome RNAi screens (two on each cell line) as described in the material and methods section. The genes with the viability difference score greater than 2 are given in the table. Additionally, UBE2N and RRM2 are included (see details in the text).

Rank	Gene	P-value	Viability difference score	Gene name
1	TXN	2.8E-05	1.50	thioredoxin
2	CFLAR	4.9E-05	2.24	CASP8 and FADD-like apoptosis regulator
3	ATAD1	5.1E-05	0.88	ATPase family, AAA domain containing 1
4	A1BG	9.9E-05	1.83	alpha-1-B glycoprotein
5	SLC16A10	1.7E-04	1.24	solute carrier family 16 (aromatic amino acid transporter), member 10
6	FAM107A	2.1E-04	0.82	family with sequence similarity 107, member A
9	RFXAP	3.3E-04	0.84	regulatory factor X-associated protein
14	CCR6	4.5E-04	2.13	chemokine (C-C motif) receptor 6

Table 2. Highest ranking genes with the lowest P-values for the effect on viability of REV3-deficient cells compared to control cells. Genes are ranked according to the P-values of the score differences for control and REV3-deficient cell lines. Only genes with P-values lower than 5E-4 and viability difference score greater than 0.8 are included.

FIGURE CAPTIONS

Figure 1. Characterization of the cell lines used in synthetic sickness/lethality screens. (*A*) REV3 mRNA level determined by rtPCR in the parental cell line A549, clone R1B6 carrying a short-hairpin RNA targeting REV3 mRNA and the control cell line S1C6 carrying a scrambled control construct. ** P <.01. Shown are means ± standard deviation (SD), n=3. (*B*) Sensitivity of the generated cell lines to continuous cisplatin (CDDP) treatment. Cell viability was determined after 5 days of CDDP treatment. Shown are means ± SD, n=3.

Figure 2. Schematic representation of the screening procedure. 24 hours after plating, cells are transfected with siRNA from the Dharmacon siARRAY human genome library targeting >20,000 transcripts. Cells are incubated for 5 days and CellTiter Blue viability assay is used to assess the number of viable cells in every well. Fluorescent signal is normalized and compared between the two cell lines – S1C6 with normal and R1B6 with reduced REV3 expression – to find the genes whose silencing predominantly affects REV3-deficient cells. The dashed line represents the hit selection threshold applied to generate the hit list shown in Table 1 (viability difference score greater than 2).

Figure 3. Inhibition of ribonucleotide reductase (RNR) expression selectively reduces number of REV3-deficient cancer cells. (*A*) Confirmation screen with siRNA pools targeting genes with high specificity for reducing cell growth of REV3 deficient cells, performed on A549, S1C6 and R1B6 cells. Data for 9 selected genes including PLK1 control are represented. Shown are means ± SD, n=3. (*B*) Quantitation of colony formation in A549 cell line after REV3 silencing by siRNA transfection and RMM1 silencing by transduction with a lentiviral vector carrying a short hairpin RNA (LV-shRRM1) at varying multiplicities of infection (MOI). Shown are means ± SD, n≥3.

Figure 4. HU treatment and REV3 silencing have synergistic growth inhibitory effect on cancer cells. (*A*) Quantitation of the colony formation after REV3 silencing by LV-shREV3 and subsequent HU treatment. Shown are means ± SD, n≥3. (*B*) Image of a representative plate from a colony formation assay after REV3 silencing by LV-shREV3 and subsequent HU treatment.

Figure 5. Effects of REV3 silencing and HU treatment on (*A*) EdU incorporation, (B) RPA2 and (*C*) γH2AX levels determined by flow cytometry . The cells were seeded and transfected the next day. After 24 hours, the medium was exchanged and after another 24 hours 0.25 mM HU was added. After 24 hours of treatment, EdU was applied for 1 hour after which cells were harvested, fixed and stained. Shown are the standard box plots representing the median with interquartile range, n≥3.

Figure 6. Effects of REV3 silencing and HU treatment on cell cycle distribution and RPA-positive cells. Panels show the percentages of cells in (*A*) G_1, (*B*) S and (*C*) G_2/M phase of the cell cycle; and the percentages RPA-positive cells in (*D*) G_1, (*E*) S and (*F*) G_2/M phase of the cell cycle. Shown are the standard box plots representing the median with interquartile range, n≥3.

Figure 7. Combination of REV3 silencing with HU-treatment induces CHK1 activation that is not accompanied by ATM phosphorylation. A549 cells were transfected and 2 days later treated with 0.25 mM HU for 24 hours. Cells treated with 2 mM HU for 80 minutes and cells irradiated with 5 Gy of γ-radiation (IR) were used as controls.

Figure 1

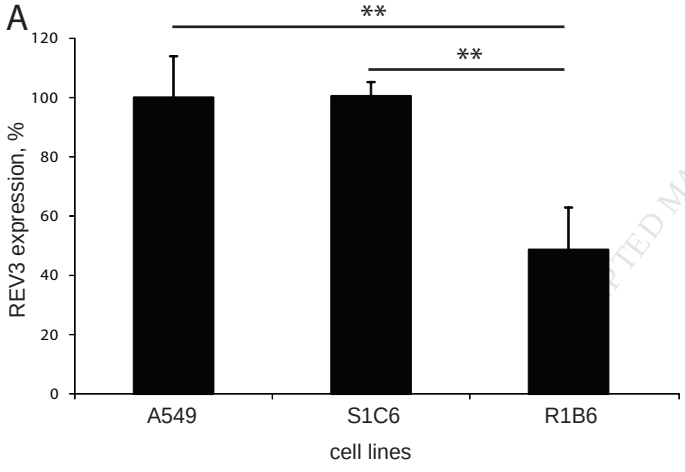

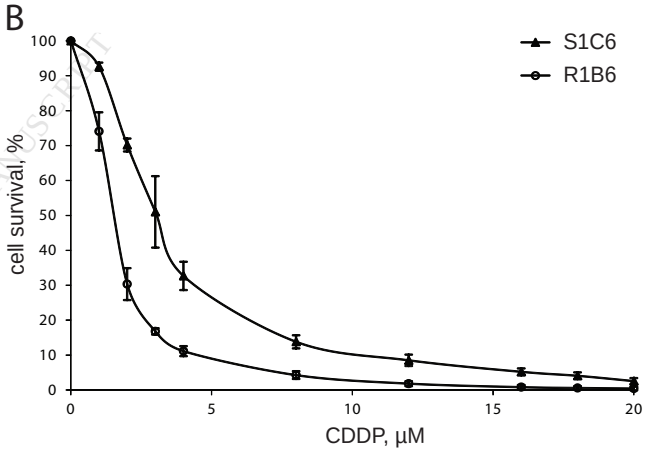

Figure 2

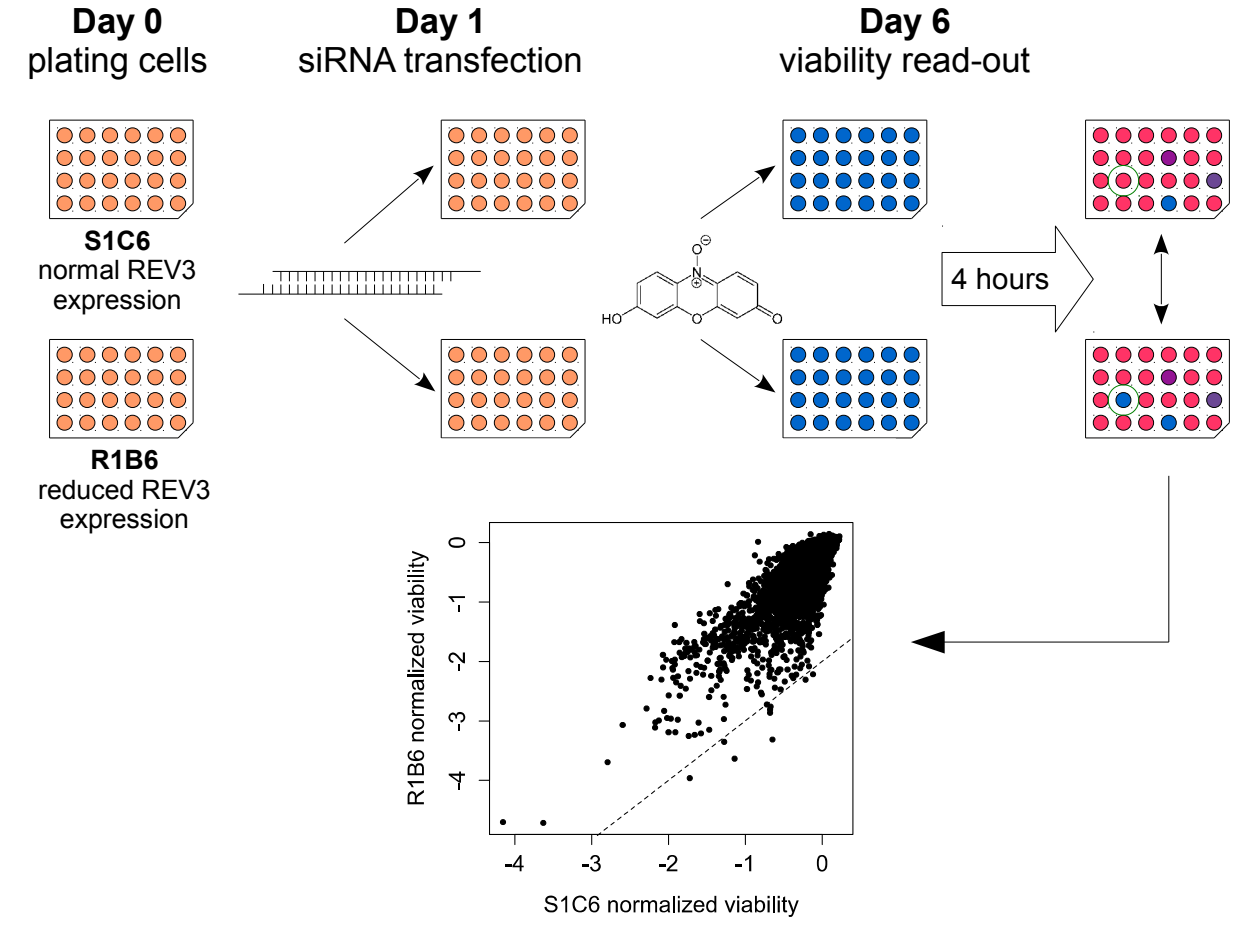
Day 0
plating cells
Day 1
siRNA transfection
Day 6
viability read-out
S1C6
normal REV3
expression
R1B6
reduced REV3
expression
HO
O
N
O
O
4 hours
R1B6 normalized viability
S1C6 normalized viability
0
-1
-2
-3
-4
-4
-3
-2
-1
0

Figure 3

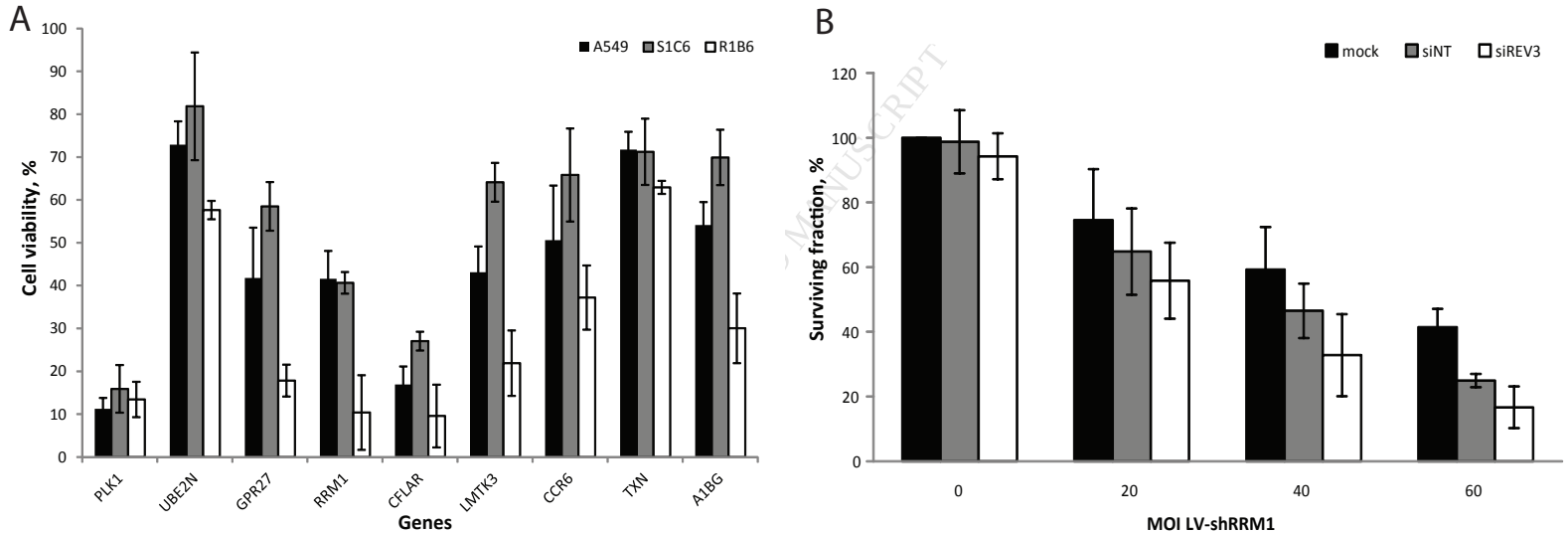

Figure 4

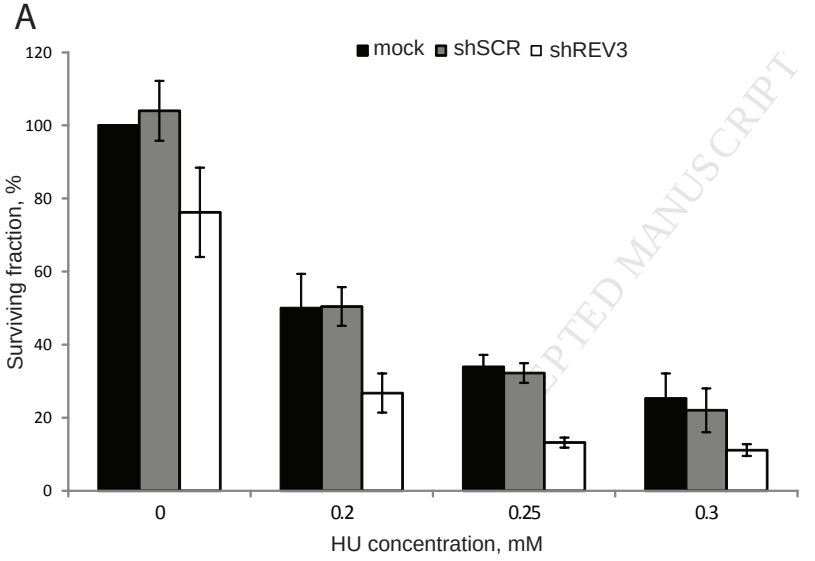

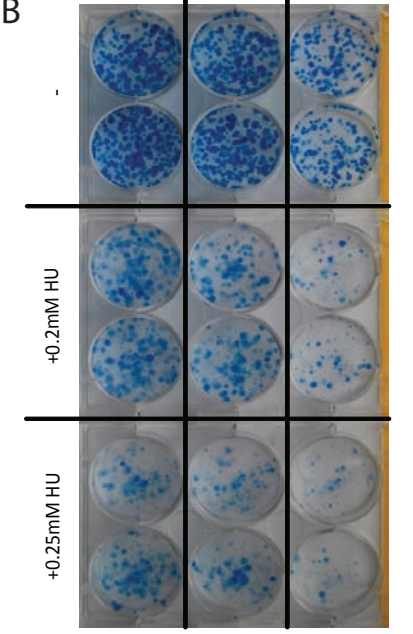

Figure 5

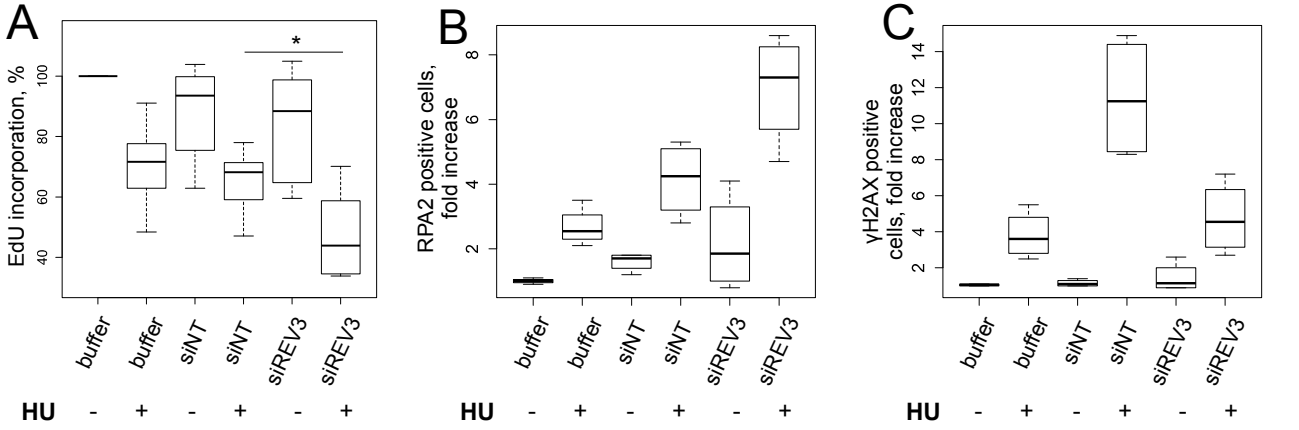
A
EdU incorporation, %
40
60
80
100
*
buffer
buffer
siNT
siNT
siREV3
siREV3
HU - + - + - +
B
RPA2 positive cells, fold increase
2
4
6
8
buffer
buffer
siNT
siNT
siREV3
siREV3
HU - + - + - +
C
γH2AX positive cells, fold increase
2
4
6
8
10
12
14
buffer
buffer
siNT
siNT
siREV3
siREV3
HU - + - + - +

Figure 6

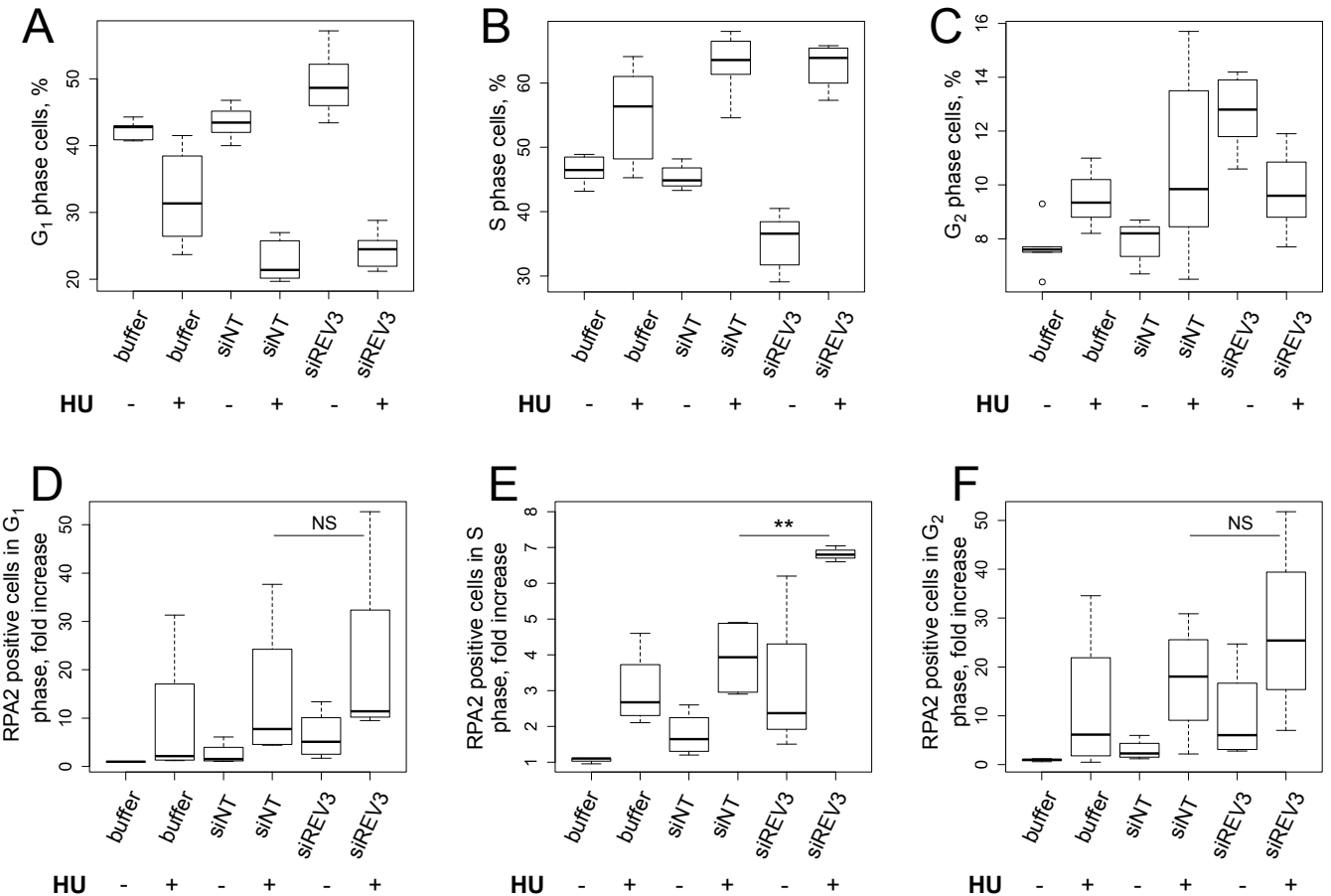
A
G1 phase cells, %
B
S phase cells, %
C
G2 phase cells, %
D
RPA2 positive cells in G1 phase, fold increase
NS
E
RPA2 positive cells in S phase, fold increase
**
F
RPA2 positive cells in G2 phase, fold increase
NS
buffer
siNT
siREV3
HU

Figure 7

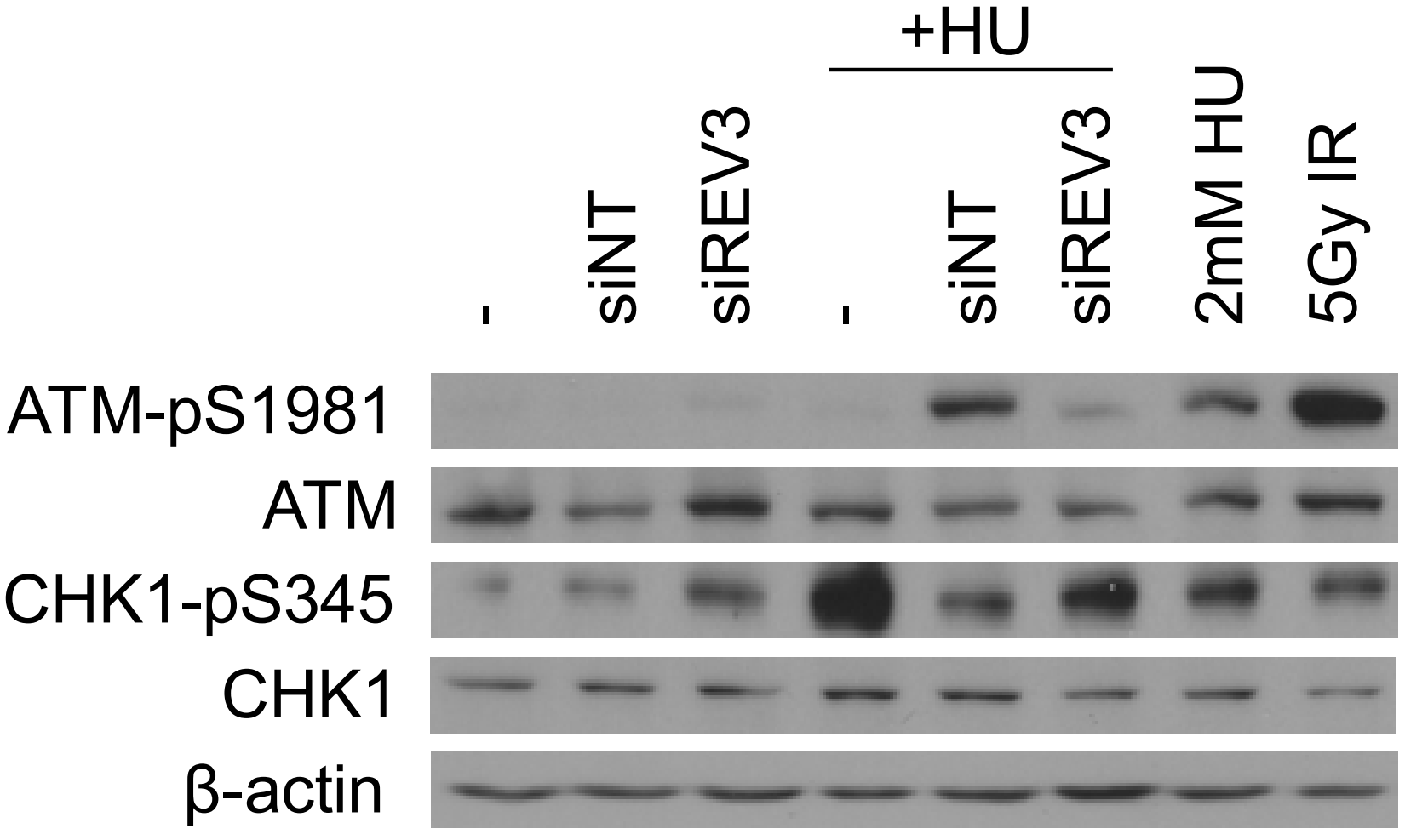
+HU
-
siNT
siREV3
-
siNT
siREV3
2mM HU
5Gy IR
ATM-pS1981
ATM
CHK1-pS345
CHK1
β-actin

Appendix A. Supplementary data

Whole genome RNAi screens reveal a critical role of REV3 in coping with replication stress

Ilya N. Kotov[a], Ellen Siebring - van Olst[b], Philip A. Knobel[a1], Ida H. van der Meulen-Muileman[c], Emanuela Felley-Bosco[a], Victor W. van Beusechem[c], Egbert F. Smit[b], Rolf A. Stahel[a] and Thomas M. Marti[a2]*

[a] Clinic of Oncology, University Hospital Zurich, 8044 Zurich, Switzerland

[b] Department of Pulmonary Diseases and [c] Department of Medical Oncology, VU University Medical Center, 1081 HV Amsterdam, the Netherlands

* Corresponding author. Clinic of Thoracic Surgery, University Hospital Bern, 3010 Bern, Switzerland. Tel: +41 31 632 40 81. Email: thomas.marti@insel.ch

[1] Present address: Institute for Research in Biomedicine, 08028 Barcelona, Spain
[2] Present address: Clinic of Thoracic Surgery, University Hospital Bern, 3010 Bern, Switzerland.

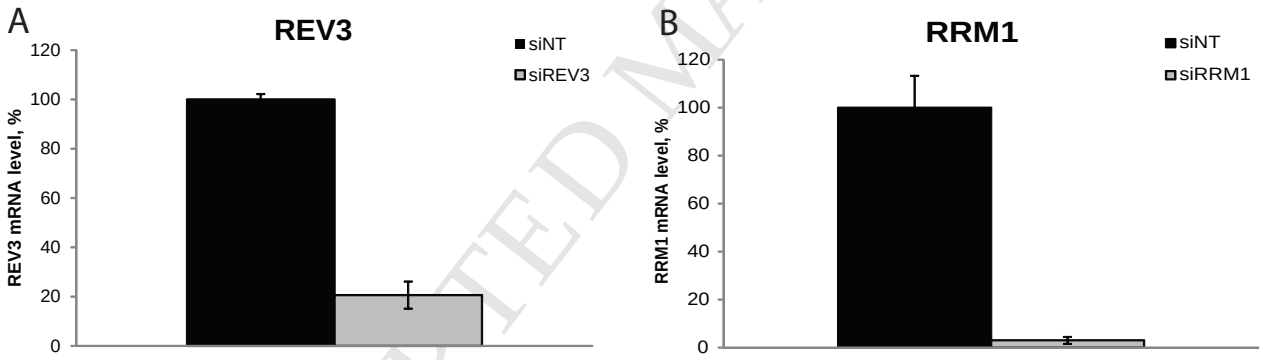

Figure A. 1. siRNA silencing results in a strong decrease of mRNA levels of (*A*) REV3 and (*B*) RRM1; 48 hours after transfection, as assessed by rtPCR. Shown are means ± SD, n=3.

	S1C6-1	S1C6-2	R1B6-1	R1B6-2
S1C6-1	1.00	0.87	0.81	0.76
S1C6-2	0.87	1.00	0.77	0.75
R1B6-1	0.81	0.77	1.00	0.84
R1B6-2	0.76	0.75	0.84	1.00

Table A. 1. Pearson's correlation values between the whole-genome silencing screens of the control (S1C6) and REV3-deficient (R1B6) cell lines.

Fig.3. Colony formation

Effect	P	
siNT	0.89172	
LVshRRM1	< 2.2e-16	***
siREV3	1.98E-06	***
siREV3:LVshRRM1	0.02423	*
siNT:LVshRRM1	0.55105	

Fig.4. Colony formation

Effect	P	
HU	< 2.2e-16	***
iREV3	2.35E-13	***
HU:iREV3	0.01848	*
LVshSCR	0.95198	
HU:LVshSCR	0.96875	

Fig.5A. EdU incorporation

Effect	P	
HU	1.46E-09	***
iREV3	0.0004234	***
HU:iREV3	0.221175	
siNT	0.0756801	.
HU:siNT	0.4750325	

Fig. 5B. RPA2

Effect	P	
HU	1.93E-06	***
iREV3	0.0055863	**
HU:iREV3	0.048098	*
siNT	0.0007516	***
HU:siNT	0.0439644	*

Fig. 5C. γH2AX

Effect	P	
HU	4.97E-07	***
iREV3	0.0018778	**
HU:iREV3	0.0008756	***
siNT	0.0078432	**
HU:siNT	0.0159109	*

Fig. 6A. G_1-phase

Effect	P	
HU	< 2.2e-16	***
iREV3	0.0132	*
HU:iREV3	0.17327	
siNT	0.01997	*
HU:siNT	5.76E-05	***

Fig. 6B. S-phase

Effect	P	
HU	3.60E-16	***
iREV3	0.0013	**
HU:iREV3	0.006225	**
siNT	0.197753	
HU:siNT	5.29E-05	***

Fig. 6C. G_2/M-phase

Effect	P	
HU	0.554353	
iREV3	0.002	**
HU:iREV3	3.92E-05	***
siNT	0.009057	**
HU:siNT	0.136432	

Fig. 6D. RPA2 in G_1-phase

Effect	P	
HU	0.04793	*
iREV3	0.42057	
HU:iREV3	0.81208	
siNT	0.29564	
HU:siNT	0.66719	

Fig. 6E. RPA2 in S-phase

Effect	P	
HU	5.71E-05	***
iREV3	0.001676	**
HU:iREV3	0.187528	
siNT	0.001701	**
HU:siNT	0.366021	

Fig. 6F. RPA2 in G_2/M-phase

Effect	P	
HU	0.01371	*
iREV3	0.17857	
HU:iREV3	0.79797	
siNT	0.15356	
HU:siNT	0.65652	

Table A. 2. Results of two-way ANOVA of experimental data. Significance codes: *** P<0.001, ** P<0.01, * P<0.05.

Gene set	P-value
Purine metabolism KEGG: hsa00230	0.0041
Pyrimidine metabolism KEGG: hsa00240	<1E-5
Replication stress [Homo sapiens]*	0.00034

Table A. 3. Selected gene sets whose silencing had stronger effect on the viability of REV3-deficient cells. We tested whether nucleotide synthesis pathways and genes associated with replication stress are enriched among the genes whose silencing had stronger effect on the viability of REV3-deficient cells. The testing was performed by ROMER. *Replication stress gene list was generated by searching NCBI gene database with the term “replication+stress” (Table A. 4).

ID	Gene	Name
7157	TP53	tumor protein p53
1029	CDKN2A	cyclin-dependent kinase inhibitor 2A
4609	MYC	v-myc myelocytomatosis viral oncogene homolog (avian)
472	ATM	ataxia telangiectasia mutated
324	APC	adenomatous polyposis coli
3320	HSP90AA1	heat shock protein 90kDa alpha (cytosolic), class A member 1
1111	CHEK1	checkpoint kinase 1
545	ATR	ataxia telangiectasia and Rad3 related
983	CDK1	cyclin-dependent kinase 1
2272	FHIT	fragile histidine triad
5591	PRKDC	protein kinase, DNA-activated, catalytic polypeptide
7486	WRN	Werner syndrome, RecQ helicase-like
898	CCNE1	cyclin E1
641	BLM	Bloom syndrome, RecQ helicase-like
3014	H2AFX	H2A histone family, member X
1025	CDK9	cyclin-dependent kinase 9
6117	RPA1	replication protein A1, 70kDa
7158	TP53BP1	tumor protein p53 binding protein 1
55294	FBXW7	F-box and WD repeat domain containing 7, E3 ubiquitin protein ligase
2177	FANCD2	Fanconi anemia, complementation group D2
83990	BRIP1	BRCA1 interacting protein C-terminal helicase 1
7465	WEE1	WEE1 homolog (S. pombe)
6118	RPA2	replication protein A2, 32kDa
5976	UPF1	UPF1 regulator of nonsense transcripts homolog (yeast)
11073	TOPBP1	topoisomerase (DNA) II binding protein 1
64421	DCLRE1C	DNA cross-link repair 1C
5424	POLD1	polymerase (DNA directed), delta 1, catalytic subunit
8317	CDC7	cell division cycle 7
9025	RNF8	ring finger protein 8, E3 ubiquitin protein ligase
571	BACH1	BTB and CNC homology 1, basic leucine zipper transcription factor 1
79840	NHEJ1	nonhomologous end-joining factor 1
5884	RAD17	RAD17 homolog (S. pombe)
10769	PLK2	polo-like kinase 2
64919	BCL11B	B-cell CLL/lymphoma 11B (zinc finger protein)
80198	MUS81	MUS81 endonuclease homolog (S. cerevisiae)
25842	ASF1A	ASF1 anti-silencing function 1 homolog A (S. cerevisiae)
55723	ASF1B	ASF1 anti-silencing function 1 homolog B (S. cerevisiae)
10116	FEM1B	fem-1 homolog b (C. elegans)
8812	CCNK	cyclin K
79915	ATAD5	ATPase family, AAA domain containing 5
80169	CTC1	CTS telomere maintenance complex component 1
4796	TONSL	tonsoku-like, DNA repair protein
84893	FBXO18	F-box protein, helicase, 18
79991	OBFC1	oligonucleotide/oligosaccharide-binding fold containing 1
84083	ZRANB3	zinc finger, RAN-binding domain containing 3
51550	CINP	cyclin-dependent kinase 2 interacting protein
92797	HELB	helicase (DNA) B
253714	MMS22L	MMS22-like, DNA repair protein

Table A. 4. Replication stress gene list, obtained by search of NCBI human gene database with the term “replication+stress”.

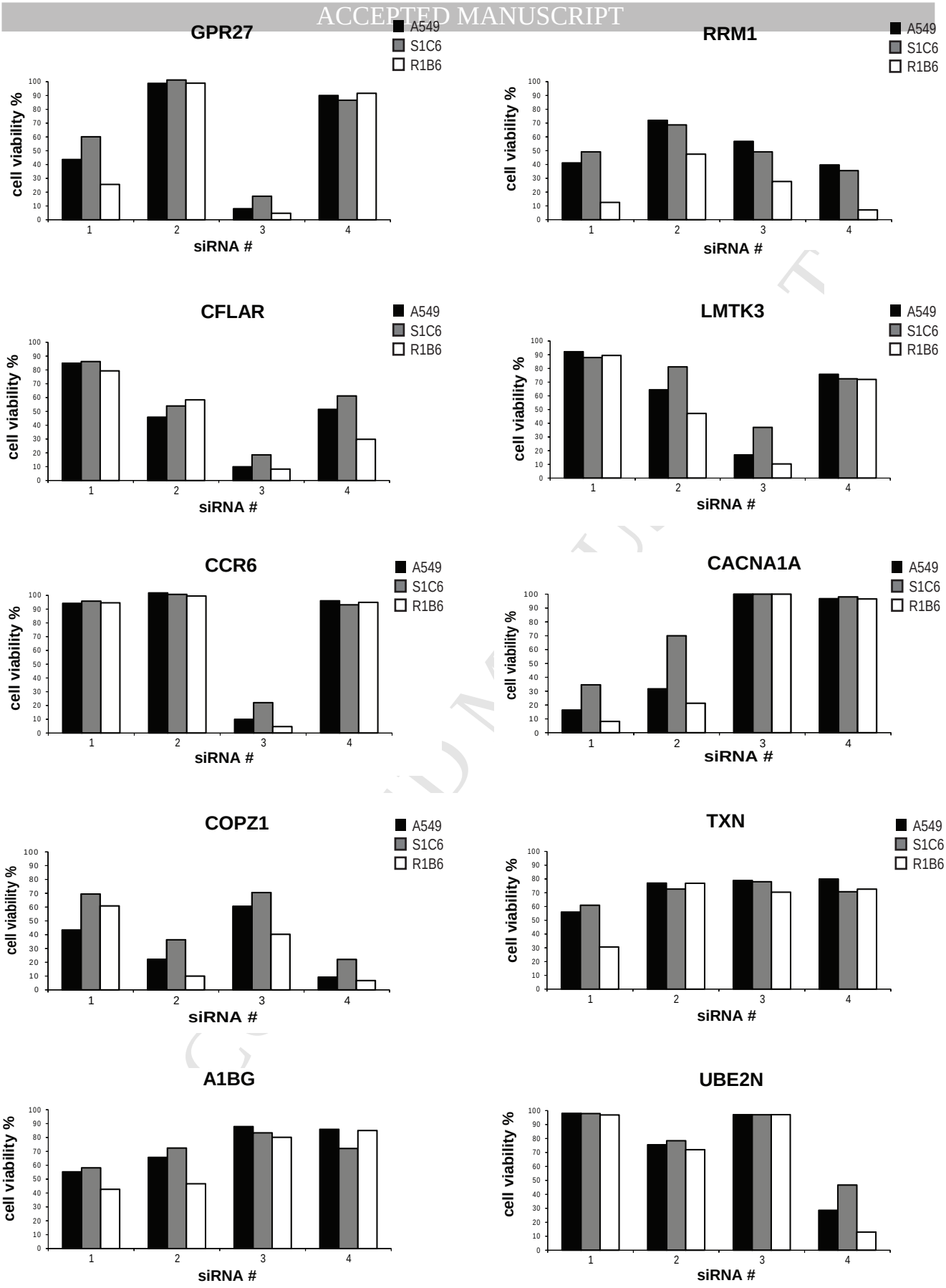

Figure A.2 Deconvolution of the siRNA pools with the highest differential viability scores in the screens. The graphs show the cell survival after transfection of each of 4 individual siRNAs. Shown are means, n=3.

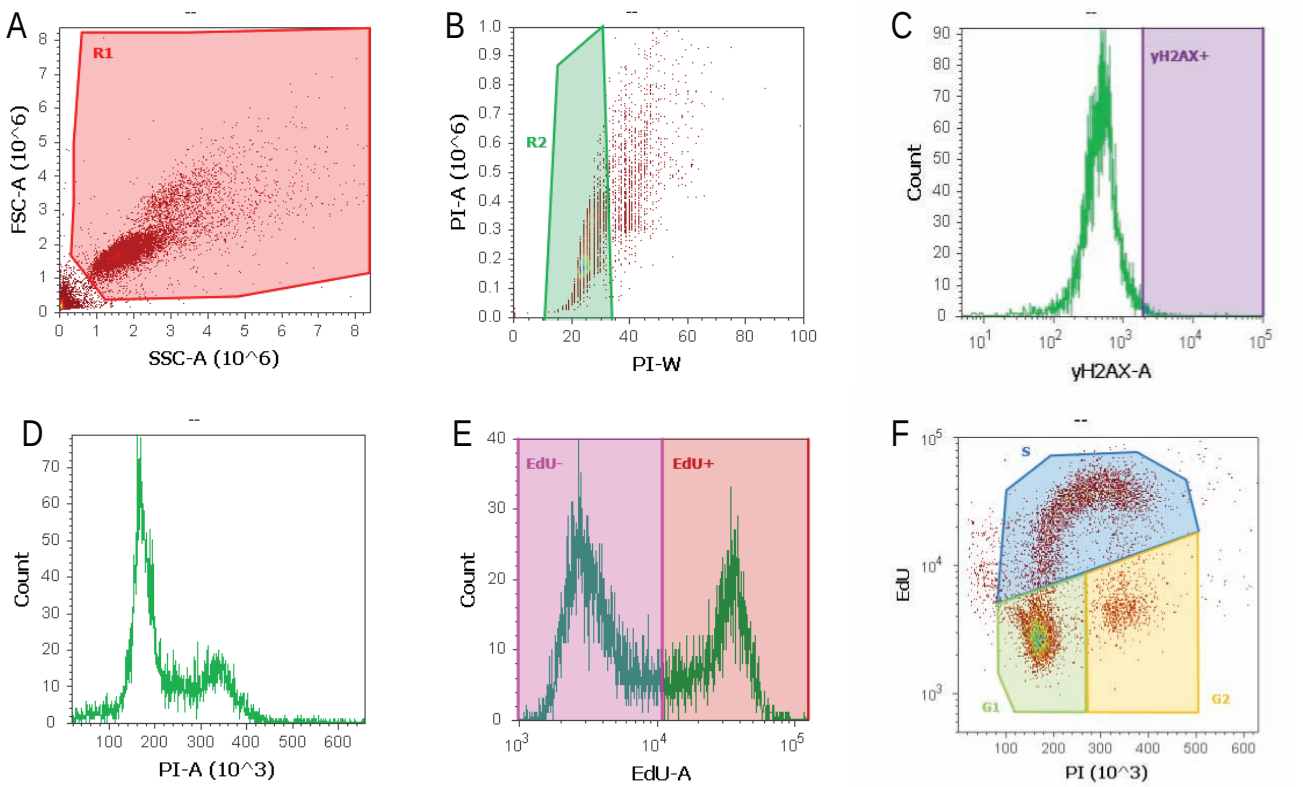

Figure A. 3. Gating strategy for the flow cytometry experiments: (*A*) exclusion of debris, (*B*) exclusion of cell douplets, (*C*) γH2AX staining, same for RPA (not shown), (*D*) PI staining, (*E*) EdU staining, (*F*) cell cycle analysis.

Polymerase	Km values, μM			
	dCTP-G	dTTP-A	dATP-T	dGTP-C
Yeast polζ	0.14 [1]	-	0.39 [2]	0.11 [1]
Yeast polδ	1.4 [3]	6.6 [3]	2.1 [3]	2.5 [3]
Yeast polη	0.43 [4]	1.3 [4]	1.7 [4]	5.0 [4]

Table A. 5. Steady-state kinetic parameters Km of yeast polymerases ζ, δ and η.

Supplemental References (Table A. 5)

1. Haracska, L., et al., *Roles of yeast DNA polymerases delta and zeta and of Rev1 in the bypass of abasic sites.* Genes Dev, 2001. **15**(8): p. 945-54.
2. Johnson, R.E., et al., *Yeast DNA polymerase zeta (zeta) is essential for error-free replication past thymine glycol.* Genes Dev, 2003. **17**(1): p. 77-87.
3. Dieckman, L.M., et al., *Pre-steady state kinetic studies of the fidelity of nucleotide incorporation by yeast DNA polymerase delta.* Biochemistry, 2010. **49**(34): p. 7344-50.
4. Washington, M.T., et al., *Fidelity and processivity of Saccharomyces cerevisiae DNA polymerase eta.* J Biol Chem, 1999. **274**(52): p. 36835-8.

Dataset B. 1. Results of the primary RNAi screens sorted by absolute difference of nor

Rank	Accession	LocusID	gene	t.stat	p.value	FDR	differentia
1	NM_018971	2850	GPR27	-9.40130222	0.00174188	0.48351905	2.666696
2	NM_001033	6240	RRM1	-4.58495536	0.01594019	0.57562388	2.494026
3	NM_003879	8837	CFLAR	-28.272544	4.88E-05	0.36223643	2.239506
4	XM_055866	114783	LMTK3	-5.0885062	0.01171657	0.57562388	2.185977
5	NM_004367	1235	CCR6	-14.2674137	0.00045462	0.4422131	2.12946
6	NM_032432	84448	ABLIM2	-1.61260015	0.19731502	0.57687699	2.095655
7	NM_000068	773	CACNA1A	-8.62504464	0.00229138	0.55038597	2.093034
8	NM_016057	22818	COPZ1	-5.47058773	0.00942725	0.57562388	2.089119
9	NM_004680	9085	CDY1	-3.95556876	0.0243616	0.57562388	2.077483
10	NM_015989	51380	CSAD	-4.08080723	0.02230413	0.57562388	2.002543
11	NM_005825	10235	RASGRP2	-5.64643689	0.00856596	0.57562388	1.929405
12	NM_001235	871	SERPINH1	-4.28180354	0.01943851	0.57562388	1.911587
13	NM_003898	8871	SYNJ2	-5.40838033	0.00975832	0.57562388	1.903974
14	XM_114621	0	LOC203076	-5.68053476	0.00841076	0.57562388	1.884617
15	NM_004831	9441	CRSP7	-4.13362149	0.02150225	0.57562388	1.851575
16	NM_194295	196968	DKFZP434I1	-2.96255391	0.05303191	0.57562388	1.844407
17	NM_198822	267020	ATP5L2	-3.45300726	0.03545878	0.57562388	1.826414
18	NM_130786	1	A1BG	-22.8019329	9.87E-05	0.41872551	1.826085
19	NM_006575	11183	MAP4K5	-4.56275375	0.01616784	0.57562388	1.795191
20	NM_002476	4635	MYL4	-2.62773602	0.07139963	0.57562388	1.78976
21	NM_007372	11325	DDX42	-6.60219185	0.00530146	0.57562388	1.768141
22	NM_020860	57620	STIM2	-12.0041722	0.00079495	0.4422131	1.728933
23	NM_033118	85366	MYLK2	-10.0228782	0.00141959	0.48351905	1.727957
24	NM_002265	3837	KPNB1	-4.283361	0.01941818	0.57562388	1.689679
25	NM_023942	65999	MGC3036	-3.79144638	0.02743295	0.57562388	1.686953
26	NM_014781	9821	RB1CC1	-6.6442483	0.00519814	0.57562388	1.679061
27	NM_001898	1469	CST1	-2.52799019	0.07830432	0.57562388	1.67029
28	NM_014691	9716	AQR	-2.3163166	0.09579444	0.57562388	1.633944
29	NM_001834	1212	CLTB	-3.16229172	0.04480737	0.57562388	1.633539
30	NM_003348	7334	UBE2N	-11.7996026	0.00084027	0.4422131	1.632375
31	NM_003278	7123	TNA	-3.42053083	0.03637459	0.57562388	1.624359
32	XM_373466	0	LOC387690	-6.63472689	0.0052213	0.57562388	1.606136
33	NM_032561	84645	C22ORF23	-9.48055205	0.00169584	0.48351905	1.60546
34	XM_372048	0	LOC389672	-13.2410241	0.00057904	0.4422131	1.601918
35	NM_003301	7201	TRHR	-4.69859912	0.01483652	0.57562388	1.591624
36	NM_006362	10482	NXF1	-1.94786259	0.13854814	0.57562388	1.574627
37	NM_014718	9746	CLSTN3	-3.10435482	0.04702074	0.57562388	1.573626
38	NM_175900	283897	FLJ35681	-4.93723055	0.01281745	0.57562388	1.573463
39	NM_002091	2922	GRP	-2.51625887	0.07916805	0.57562388	1.571913
40	NM_014338	23761	PISD	-4.12031145	0.02170087	0.57562388	1.569932
41	NM_012152	23566	EDG7	-8.52883436	0.00237437	0.55902722	1.556974
42	NM_001063	7018	TF	-5.29569096	0.01039681	0.57562388	1.525556
43	NM_003806	8739	HRK	-2.67089585	0.06864053	0.57562388	1.525383
44	NM_001776	953	ENTPD1	-11.1028897	0.0010222	0.48196901	1.517526
45	NM_020882	57642	KIAA1510	-4.8080603	0.01386363	0.57562388	1.515316
46	NM_000937	5430	POLR2A	-4.91556246	0.01298575	0.57562388	1.515048
47	NM_021138	7186	TRAF2	-1.83262757	0.15618404	0.57562388	1.506787
48	NM_003329	7295	TXN	-33.5783272	2.78E-05	0.36223643	1.502514
49	NM_018438	26270	FBXO6	-3.07077742	0.04836516	0.57562388	1.501946
50	NM_017986	55065	FLJ10060	-3.40139197	0.03692807	0.57562388	1.501052
51	NM_030651	80863	C6ORF31	-5.46438253	0.00945963	0.57562388	1.493475
52	NM_006421	10565	BIG1	-11.8308746	0.00083313	0.4422131	1.485841
53	NM_020861	57621	ZBTB2	-7.43644879	0.00365829	0.57562388	1.480462

54	NM_004462	2222	FDFT1	-5.83647831	0.00774513	0.57562388	1.470012
55	NM_001492	2657	GDF1	-2.63675476	0.07081219	0.57562388	1.46846
56	XM_290811	80816	KIAA1713	-5.74797719	0.00811424	0.57562388	1.44717
57	NM_002455	4580	MTX1	-1.72566142	0.17484922	0.57562388	1.431868
58	NM_001015	6205	RPS11	-2.70797113	0.06637267	0.57562388	1.420874
59	XM_016548	203611	CDY	-2.8259668	0.05973521	0.57562388	1.420741
60	NM_000832	2902	GRIN1	-4.27150969	0.01957357	0.57562388	1.419661
61	NM_014207	921	CD5	-4.23608314	0.02004751	0.57562388	1.418187
62	NM_015470	26056	GAF1	-2.04238114	0.12576869	0.57562388	1.404183
63	NM_012318	3954	LETM1	-1.8765361	0.14917966	0.57562388	1.400908
64	NM_001318	1444	CSHL1	-3.85696037	0.02615177	0.57562388	1.393769
65	NM_001153	307	ANXA4	-6.81486949	0.00480461	0.57562388	1.391089
66	NM_014261	148022	TRIF	-3.34138669	0.03873248	0.57562388	1.372367
67	NM_001679	483	ATP1B3	-4.27153073	0.01957329	0.57562388	1.355509
68	XM_084445	0	LOC143158	-2.98769674	0.05190017	0.57562388	1.345385
69	NM_014293	23467	NPTXR	-2.15248569	0.11256347	0.57562388	1.334069
70	NM_016564	51286	BM88	-3.35160412	0.03841764	0.57562388	1.327834
71	NM_021974	5435	POLR2F	-5.15746533	0.01125474	0.57562388	1.324421
72	NM_005227	1945	EFNA4	-2.94870315	0.05366827	0.57562388	1.322891
73	XM_171060	253639	ZNF620	-2.98942432	0.05182349	0.57562388	1.319373
74	NM_007366	22925	PLA2R1	-1.90267617	0.14517907	0.57562388	1.315942
75	NM_016451	1315	COPB	-6.05761956	0.00691252	0.57562388	1.313703
76	NM_018489	55870	ASH1L	-3.66636985	0.03010497	0.57562388	1.312102
77	NM_017836	54946	SLC41A3	-2.82474999	0.05979943	0.57562388	1.306341
78	NM_016265	51711	ZNF325	-5.46897849	0.00943564	0.57562388	1.290793
79	NM_006083	3550	IK	-1.55011729	0.21107258	0.57815733	1.281843
80	NM_197964	154791	HSPC268	-7.09941456	0.00422968	0.57562388	1.277608
81	NM_005649	6940	ZNF354A	-12.97474	0.00061838	0.4422131	1.274754
82	XM_047083	0	LOC92755	-5.22650515	0.01081538	0.57562388	1.271161
83	NM_023016	65124	C2ORF26	-4.58047237	0.01598583	0.57562388	1.262959
84	NM_024080	79054	TRPM8	-5.68480042	0.00839159	0.57562388	1.261654
85	NM_022567	60506	NYX	-2.44227707	0.08488551	0.57562388	1.261258
86	NM_024110	79092	CARD14	-4.38344954	0.01816612	0.57562388	1.260132
87	NM_080622	140701	C20ORF135	-3.26487621	0.04119461	0.57562388	1.259969
88	NM_003412	7545	ZIC1	-5.69805753	0.0083324	0.57562388	1.257849
89	XM_371488	0	LOC388939	-3.80604727	0.02714073	0.57562388	1.256481
90	NM_021126	4357	MPST	-2.48506252	0.08152102	0.57562388	1.25445
91	NM_001386	1808	DPYSL2	-1.79513373	0.16245974	0.57562388	1.253711
92	XM_116971	196993	LOC196993	-5.99521954	0.00713533	0.57562388	1.249537
93	NM_007346	11054	OGFR	-2.04389282	0.12557562	0.57562388	1.243349
94	NM_018593	117247	SLC16A10	-19.4232316	0.0001666	0.4422131	1.238147
95	NM_021251	11132	CAPN10	-9.91634157	0.00146898	0.48351905	1.235937
96	NM_016202	51157	ZNF580	-4.24964459	0.01986439	0.57562388	1.234412
97	NM_000813	2561	GABRB2	-2.45012084	0.08425647	0.57562388	1.229346
98	NM_022304	3274	HRH2	-2.96054945	0.05312343	0.57562388	1.2278
99	NM_004545	4707	NDUFB1	-2.28057738	0.09918687	0.57562388	1.224029
100	NM_020348	26507	CNNM1	-5.85645855	0.00766479	0.57562388	1.214948
101	NM_014665	9684	LRRC14	-2.1628459	0.11140613	0.57562388	1.213947
102	NM_006233	5438	POLR2I	-3.79511793	0.0273591	0.57562388	1.207967
103	NM_003427	7629	ZNF76	-7.46438207	0.00361552	0.57562388	1.207862
104	NM_015319	23371	TENC1	-2.27547182	0.09968299	0.57562388	1.207848
105	NM_017990	55066	PDPR	-2.66570027	0.06896577	0.57562388	1.207647
106	XM_379840	0	LOC402509	-1.99226053	0.13236811	0.57562388	1.206983
107	NM_004390	1512	CTSH	-9.72230391	0.0015648	0.48351905	1.206209
108	NM_174925	205251	LOC205251	-1.61282562	0.19726718	0.57687699	1.202894
109	NM_014569	23660	ZFP95	-3.63808964	0.03075364	0.57562388	1.199439

110	NM_000687	191	AHCY	-8.34814439	0.00254103	0.55902722	1.196668
111	XM_379501	0	LOC401367	-3.80278079	0.02720576	0.57562388	1.195346
112	NM_022751	64762	C18ORF11	-2.63693947	0.07080022	0.57562388	1.193569
113	NM_001655	372	ARCN1	-2.95930319	0.05318043	0.57562388	1.192574
114	NM_002140	3190	HNRPK	-1.67582881	0.18438349	0.57562388	1.191434
115	NM_017776	55634	FLJ20344	-2.79877068	0.06119076	0.57562388	1.191049
116	NM_078483	206358	SLC36A1	-4.25959507	0.01973137	0.57562388	1.185451
117	NM_006462	10616	C20ORF18	-1.67075795	0.18538545	0.57562388	1.181995
118	NM_015305	23357	KIAA0759	-4.51726915	0.01664724	0.57562388	1.177352
119	NM_001535	3275	HRMT1L1	-3.63869781	0.03073951	0.57562388	1.177119
120	NM_198504	344838	PAQR9	-3.90083673	0.02533551	0.57562388	1.175835
121	NM_016305	51188	SS18L2	-3.46051434	0.03525117	0.57562388	1.169052
122	NM_002594	5126	PCSK2	-2.96625187	0.05286357	0.57562388	1.165381
123	NM_198401	157567	LOC157567	-2.29361856	0.0979328	0.57562388	1.15347
124	NM_002951	6185	RPN2	-4.2776666	0.01949265	0.57562388	1.150616
125	NM_006253	5564	PRKAB1	-1.56186399	0.2084088	0.57815733	1.149823
126	NM_020847	27327	TNRC6	-4.96675671	0.01259255	0.57562388	1.146274
127	NM_022156	64118	PP3111	-2.28145635	0.09910176	0.57562388	1.145053
128	NM_003951	9016	SLC25A14	-1.46238852	0.23216203	0.57827016	1.131503
129	NM_014033	25840	DKFZP586A	-4.23024689	0.02012698	0.57562388	1.127486
130	NM_002434	4350	MPG	-2.64846459	0.07005813	0.57562388	1.127265
131	NM_004500	3183	HNRPC	-1.24510371	0.29450435	0.59440153	1.126523
132	NM_031309	83482	SCRT1	-4.61941634	0.01559483	0.57562388	1.119456
133	NM_001762	908	CCT6A	-10.3758286	0.00127059	0.48351905	1.115444
134	NM_014632	9645	MICAL2	-1.49889769	0.22312365	0.57815733	1.114972
135	NM_178858	118980	SFXN2	-5.20676911	0.01093871	0.57562388	1.114772
136	NM_145255	124995	MRPL10	-4.27088466	0.0195818	0.57562388	1.113375
137	NM_023068	6614	SN	-2.83063494	0.05948962	0.57562388	1.112715
138	NM_002826	5768	QSCN6	-2.23004916	0.10422787	0.57562388	1.110032
139	NM_024763	79819	FLJ23129	-3.06810863	0.04847403	0.57562388	1.109393
140	NM_130807	126308	MOBKL2A	-4.90361462	0.01307976	0.57562388	1.107674
141	NM_021620	59336	PRDM13	-1.8137446	0.15930989	0.57562388	1.105833
142	NM_015004	23016	EXOSC7	-2.04695013	0.12518619	0.57562388	1.103749
143	NM_024627	79680	FLJ21125	-2.07443711	0.12174701	0.57562388	1.100817
144	XM_380120	0	LOC402537	-3.91332864	0.02510898	0.57562388	1.100767
145	NM_144639	131669	FLJ31300	-5.53303853	0.0091092	0.57562388	1.093867
146	NM_002068	2769	GNA15	-4.31370168	0.01902742	0.57562388	1.090654
147	XM_371501	200424	MGC22014	-2.40138711	0.08825678	0.57562388	1.090504
148	NM_015642	26137	ZNF288	-2.08669924	0.12024813	0.57562388	1.08555
149	NM_021009	7316	UBC	-8.39703059	0.00249449	0.55902722	1.085506
150	NM_003002	6392	SDHD	-1.70681852	0.17838861	0.57562388	1.074185
151	NM_017534	4620	MYH2	-8.45971107	0.00243641	0.55902722	1.070938
152	NM_001299	1264	CNN1	-1.45831629	0.23319405	0.57836885	1.068407
153	NM_002419	4296	MAP3K11	-4.2569195	0.01976703	0.57562388	1.068129
154	NM_004062	1014	CDH16	-2.43842145	0.08519676	0.57562388	1.067915
155	NM_024031	78994	MGC3121	-3.09888164	0.04723672	0.57562388	1.064762
156	NM_003311	7262	PHLDA2	-1.78268786	0.16460517	0.57562388	1.064221
157	NM_031421	83538	DKFZP434H	-2.29483934	0.09781636	0.57562388	1.057592
158	NM_004741	9221	NOLC1	-2.24000078	0.10321163	0.57562388	1.057478
159	NM_002645	5286	PIK3C2A	-4.9645125	0.01260946	0.57562388	1.055754
160	NM_013265	738	C11ORF2	-1.60521498	0.19888909	0.57687699	1.054983
161	NM_152544	152992	FLJ23861	-1.74649826	0.1710259	0.57562388	1.049267
162	NM_207477	400931	FLJ27365	-3.74661682	0.02835516	0.57562388	1.048371
163	NM_031287	83443	SF3B5	-2.17542124	0.11001995	0.57562388	1.042922
164	NM_014325	23603	CORO1C	-3.36723109	0.03794221	0.57562388	1.041365
165	NM_006645	10809	STARD10	-1.8128112	0.15946623	0.57562388	1.040594